

Air-sea flux of oxygen estimated from bulk data: Implications for the marine and atmospheric oxygen cycles

Nicolas Gruber,¹ Manuel Gloor,² Song-Miao Fan, and Jorge L. Sarmiento

Atmospheric and Oceanic Sciences Program, Princeton University, Princeton, New Jersey, USA

Abstract. We estimate the annual net air-sea fluxes of oxygen for 13 regions on the basis of a steady state inverse modeling technique that is independent of air-sea gas exchange parameterizations. The inverted data consist of the observed oceanic oxygen concentration after a correction has been applied to account for biological cycling. We find that the tropical oceans (13°S–13°N) emit $\sim 212 \text{ Tmol O}_2 \text{ yr}^{-1}$, which is compensated by uptake of 148 Tmol yr^{-1} in the Northern Hemisphere ($>13^\circ\text{N}$) and by uptake of 65 Tmol yr^{-1} in the Southern Hemisphere ($<13^\circ\text{S}$). These results imply that the dominant feature of oxygen transport in the combined ocean-atmosphere system is the existence of a closed circulation cell in each hemisphere. These two cells consist of O_2 uptake by the ocean in the middle and high latitudes of both hemispheres and transport in the ocean toward the tropics, where O_2 is lost to the atmosphere and transported in the atmosphere back toward the poles. We find an asymmetry in the two cells involving O_2 uptake in the temperate regions of the Northern Hemisphere versus loss of O_2 in the temperate regions of the Southern Hemisphere. There is an additional asymmetry between the Atlantic basin, which has a net southward transport at all latitudes north of 36°S , in agreement with independent transport estimates, versus the Indian and Pacific Oceans, which have a strong equatorward transport everywhere. We find that these inverse estimates are relatively insensitive to details in the inversion scheme but are sensitive to biases in the ocean general circulation model that provides the linkage between surface fluxes and ocean interior concentrations. Forward simulations of O_2 in an atmospheric tracer transport model using our inversely estimated oxygen fluxes as a boundary condition agree reasonably well with observations of atmospheric potential oxygen ($\text{APO} \approx \text{O}_2 + \text{CO}_2$). Our results indicate that the north–south asymmetry in the strength of the two hemispheric cells coupled with a strong asymmetry in fossil fuel emissions can explain much of the observed interhemispheric gradient in APO. Therefore it might not be necessary to invoke the existence of a large southward interhemispheric transport of O_2 in the ocean, such as proposed by *Stephens et al.* [1998]. However, we find that uncertainties in the modeled APO distribution stemming from seasonal atmospheric rectification effects and the limited APO data coverage prevent the currently available APO data from providing strong constraints on the magnitude of interhemispheric transport.

1. Introduction

Measurements of variations in atmospheric oxygen have provided a wealth of insights into the global carbon cycle [*Keeling and Shertz*, 1992; *Keeling et al.*, 1993, 1996; *Bender et al.*, 1996; *Battle et al.*, 2000]. This is because atmospheric oxygen is in many respects a mirror of atmospheric CO_2 , caused by the tight link between O_2 and CO_2 that occurs during the photosynthesis by land plants and the subsequent respiration and remineralization of terrestrial organic matter [*Severinghaus*, 1995]. Since fossil fuels consist of ancient organic matter, a similar tight stoichiometric relation exists for the burning of fossil fuels, although with a slightly higher oxygen to carbon exchange ratio (-1.4 instead of -1.1) [*Keeling and Shertz*, 1992]. In addition to terrestrial

exchange processes, atmospheric O_2 is also influenced by the exchange of oxygen across the air-sea interface.

Stephens et al. [1998] recently proposed a new tracer combination, atmospheric potential oxygen ($\text{APO} \sim \text{O}_2 + \text{CO}_2$), that removes the terrestrial influence from the atmospheric O_2 signal, including most of the signal from the burning of fossil fuels. Variations in APO therefore reflect mainly the air-sea exchange of oxygen and, to a smaller degree, also the air-sea exchange of CO_2 , N_2 , and a residual signal from the burning of fossil fuels. Annual mean observations of APO from 10 stations along a north–south transect show a significant interhemispheric gradient of APO with concentrations decreasing toward the north. *Stephens et al.* [1998] used this tracer to evaluate three global ocean carbon cycle models with regard to their simulations of O_2 , CO_2 , and N_2 fluxes across the air-sea interface. When they combined these fluxes with an atmospheric transport model, they found that all models significantly underestimated the interhemispheric gradient in APO. They interpreted this shortcoming as the result of an underestimation of the southward transport of the sum of O_2 and CO_2 in the oceans. They suspected that the excessive heat flux out of the Southern Ocean, caused by inadequate parameterizations of subgrid-scale eddy mixing, vertical mixing, and sea ice formation and an over-

¹Now at University of California, Los Angeles, Los Angeles, California, USA.

²Now at Max Planck Institute of Biogeochemistry, Jena, Germany.

estimation of the vertical diffusivity in the main thermocline, might be the primary reasons for this deficiency.

However, simulations by *Aumont* [1998], using a three-dimensional (3-D) ocean carbon cycle model with much lower vertical diffusivity and significantly lower heat loss in the Southern Ocean, still failed to reproduce the interhemispheric gradient in APO, suggesting that other processes, such as atmospheric transport model errors, might cause the model-data discrepancy. One possibility is the existence of seasonal rectifier effects [Denning *et al.*, 1995] that can cause the annual mean APO concentration to be "rectified" toward higher or lower values as a consequence of seasonal covariation between fluxes and transport. *Stephens* [1999] discusses the possibility of the existence of such a rectifier effect for APO at the South Pole station, which causes this location to have substantially higher annual average APO concentrations than stations located within the marine boundary layer. This rectification might be the result of the observation that air at the South Pole station originates in the summer predominantly from the marine boundary layer over the Southern Ocean, whereas the South Pole station is essentially blocked from this marine boundary layer air in winter as a result of the strong Antarctic inversion. Since the marine boundary air over the Southern Ocean has high O₂ concentrations in the summer and low O₂ concentration in the winter [Keeling *et al.*, 1998], the annual average APO concentration at the South Pole could be rectified toward higher APO relative to a marine boundary station close to the Southern Ocean. As shown by *Stephens et al.* [1998], seasonal APO rectification effects can also arise in temperate and subpolar latitudes, where strong seasonality in the exchange of O₂ and CO₂ between the ocean and the atmosphere can covary with seasonal changes in the depth of the marine boundary layer. The exact magnitude of such atmospheric rectification effects is currently relatively poorly understood and subject of an intense debate [Denning *et al.*, 1995]. It is also one of the areas where atmospheric transport models strongly disagree with each other [Law *et al.*, 1996; Denning *et al.*, 1999], introducing substantial uncertainties in the modeled distribution of tracers in the atmosphere. These uncertainties introduced by atmospheric transport models therefore limit the strength of the constraint that APO observations can impose on large-scale oceanic transport of oxygen.

An alternative means to test the models would be to compare the model-simulated fluxes directly against observed fluxes of O₂ and CO₂, eliminating the need for an atmospheric transport model. While global compilations for air-sea CO₂ partial pressure differences have made it possible to compute climatological maps of CO₂ fluxes [Takahashi *et al.*, 1997, 1999], corresponding compilations for oxygen have been hampered by data scarcity and the fact that relative undersaturation and supersaturations of O₂ at the air-sea interface are about an order of magnitude smaller than those for CO₂. This is because an oxygen anomaly in the ocean equilibrates ~10 times faster with the atmosphere than a CO₂ anomaly [Broecker and Peng, 1974]. Therefore a much higher precision in the determination of O₂ partial pressure differences and also a denser sampling is required for O₂ in order to reliably record spatiotemporal variability. A first attempt to generate such a compilation for O₂ was made by *Najjar and Keeling* [1997] on the basis of historical data archived at the National Oceanographic Data Center. Their focus was on the seasonal cycle. However, basin-scale to interhemispheric transport is primarily governed by the net flux over the annual period. Since most of the oxygen signal is seasonal, the data requirements for obtaining annual net fluxes from observations are extremely large. *Najjar and Keeling* [1999] used the compilation of *Najjar and Keeling* [1997] for investigating annual net fluxes of O₂, but many uncertainties and potential biases are associated with these estimates, not the least of these being the uncertainties due to the parameterization of air-sea gas exchange [Wanninkhof, 1992; Liss and Merlivat, 1986; Wanninkhof and McGillis, 1999].

We propose here a new, alternative method to estimate annual net air-sea fluxes of O₂. This estimation is done by means of an inversion of the oceanic oxygen field after correcting it for biological processes. This approach does not rely on assumptions about the parameterization of air-sea gas exchange, nor does it require knowledge of the air-sea partial pressure difference for O₂. The only assumptions made are that the ocean transport is known sufficiently well and that biological processes affect the distribution of oxygen and nutrients in a constant stoichiometric ratio. We extensively tested our method using modeled and observed temperatures to estimate heat fluxes [Gloor *et al.*, this issue]. These tests showed that this inversion method is generally successful in retrieving the fluxes from the observed tracer distribution, but that model circulation biases can introduce substantial uncertainties. *Gloor et al.* [this issue] nevertheless demonstrated that the estimated heat fluxes are of about equal quality as present heat flux climatologies based on surface ocean observations. We conclude from these results that our oxygen inversion estimates are reasonably realistic but that the accuracy of the results is limited by deficiencies in the ocean circulation models. It is therefore important to note that the O₂ fluxes estimated by this method are not independent of the characteristics of the underlying OGCM. However, our inversion method allows us to estimate oxygen fluxes independently of an ocean biogeochemical model and therefore provides an important constraint on how biological cycling of O₂ and its interaction with the ocean circulation is represented in such biogeochemical models.

We will describe the concept of the oxygen inversion method in section 2. Afterward, in section 3, we will provide the details of this oceanic inversion. The results are presented and discussed in section 4. We will then investigate the implications of these fluxes for atmospheric APO in section 5 and summarize the results of this study in section 6 together with our conclusions.

2. Concept

Our method is based on the fact that net air-sea fluxes of O₂ lead to net changes in the ocean oxygen concentration and that these changes are preserved once a water parcel loses contact with the atmosphere. The full preservation of the gas exchange signal is prevented by the production and consumption of oxygen in the water by photosynthesis, respiration, and remineralization. However, these biological processes consume and release phosphate at the same time with a relatively constant stoichiometry relative to O₂. This permits us to correct the ocean oxygen concentrations for the influence of these biological processes by defining a tracer O₂^{*} that is observed to reflect just the air-sea exchange of O₂:

$$O_2^* = O_2 - r_{O_2:PO_4} PO_4, \quad (1)$$

where $r_{O_2:PO_4}$ is the stoichiometric O₂ to PO₄ ratio during marine photosynthesis, respiration, and remineralization, taken to be -170 according to *Anderson and Sarmiento* [1994]. All concentrations in (1) are salinity normalized in order to make O₂^{*} conservative with respect to the addition or removal of freshwater at the ocean's surface. If the assumption about the constant stoichiometric ratio is correct, then O₂^{*} has no sources and sinks in the interior of the ocean (conservative tracer) and just reflects the addition or removal of O₂ by air-sea gas exchange [Keeling and Peng, 1995]. Note that O₂^{*} is equivalent to the tracers PO [Broecker and Peng, 1974] and PO₄^{*} [Broecker *et al.*, 1991], except that O₂^{*} is expressed in units of oxygen.

Two oceanic processes can cause air-sea disequilibrium of oxygen and thus lead to air-sea fluxes. First, heat and freshwater fluxes alter the solubility of oxygen in seawater, and second, biological production and consumption add or remove oxygen from the water. The importance of these two processes becomes clear by inspect-

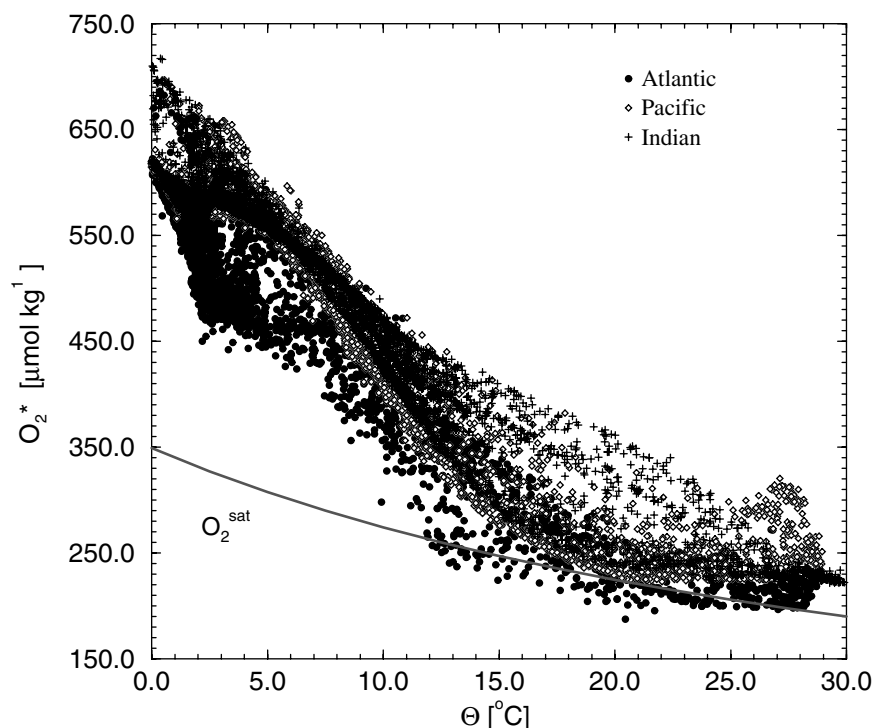


Figure 1. Scatterplot of O_2^* versus potential temperature. Shown are data from all depths and from selected cruises in the Atlantic (South Atlantic Ventilation Experiment (SAVE), National Oceanic and Atmospheric Administration (NOAA)/Atlantic Oceanographic and Meteorological Laboratory (AOML) North Atlantic 1993 cruise), in the Pacific (World Ocean Experiment (WOCE) cruise P16), and in the Indian Oceans (WOCE I9N18S). The line shows the temperature dependence of the O_2 solubility.

ing Figure 1, which shows a scatterplot of O_2^* versus potential temperature. The tracer O_2^* is strongly negatively correlated with potential temperature. This is as expected since the oxygen saturation concentration increases with decreasing temperatures (line in Figure 1). However, the O_2^* variations that are associated with the temperature dependence of oxygen saturation (thermal component) can only explain about a third of the O_2^* covariation with temperature. Since salinity variations are relatively small, the influence of freshwater on O_2^* variations are small as well. Therefore the remaining fraction of the O_2^* covariation, i.e., the difference between O_2^* and the solubility curve, must reflect the impact of biological processes on the O_2 air-sea gas exchange (biological component). It is noteworthy that the difference between O_2^* and the O_2 solubility (i.e., the biological component) is larger at low temperatures and smaller at high temperatures. This means that as one moves from the low latitudes to high latitudes, waters generally gain O_2 from the atmosphere because of both increased solubility (colder temperatures) and biology. Figure 1 therefore suggests that the thermal and biological components have a tendency to act in the same direction. Results from our inversion will demonstrate that this is indeed the case.

Once O_2^* has been calculated, net air-sea fluxes of O_2 can be estimated by combining spatial gradients in O_2^* with estimates of how fast waters flow into and out of a given surface region and by assuming steady state. This is because O_2^* conservation requires that the air-sea flux is equal to the water mass flow times the O_2^* difference between the inflowing and outflowing waters. Figure 2 shows this principle for the central Pacific. Concentrations of O_2^* in the waters feeding the equatorial upwelling have relatively high O_2^* concentrations. This is mainly a consequence of these waters being cooler than the surface waters. As these waters upwell to the surface, they lose oxygen to the atmosphere owing to warming and

also to the production of excess O_2 from net biological production. This outgassing of oxygen lowers O_2^* from $\sim 400 \mu\text{mol kg}^{-1}$ to $280 \mu\text{mol kg}^{-1}$. Assuming that this O_2^* loss is representative of the entire upwelling region in the equatorial Pacific (3°S – 3°N , 180°W – 90°W) and adopting an upwelling of 40 sverdrups (Sv) [Johnson, 2001; Wanninkhof et al., 1995; Lefèvre et al., 1994; Broecker and Peng, 1982] yield an estimated oxygen loss of $\sim 150 \text{ Tmol } O_2 \text{ yr}^{-1}$ ($1 \text{ Tmol} = 10^{12} \text{ mol}$). This simple estimate is highly uncertain because the upwelling in the equatorial Pacific is not well known but is in good agreement with our inversion results reported below.

Rather than estimating water mass transport rates for many regions individually, we employ a 3-D ocean general circulation model (OGCM) and a steady state inversion scheme to estimate the air-sea fluxes of O_2 over the entire surface of the ocean. We will explain this method in more detail in section 3.

3. Methods

We use a steady state inversion scheme first used by Bolin and Keeling [1963] and later widely adopted to invert atmospheric CO_2 observations [Enting and Mansbridge, 1989; Keeling et al., 1989; Fan et al., 1998] in order to estimate annual net air-sea fluxes of O_2 from the oceanic distribution of O_2^* . This inversion method relies on the linearity of the tracer continuity equation, which makes it possible to decompose an observed concentration field into contributions from different regional sources. We will briefly summarize the method here. The reader interested in more details regarding the mathematical aspects is referred to Gloor et al. [2000] and Fan et al. [1999], and those interested in the specific adaptations for performing oceanic inversions are referred to Gloor et al. [this issue].

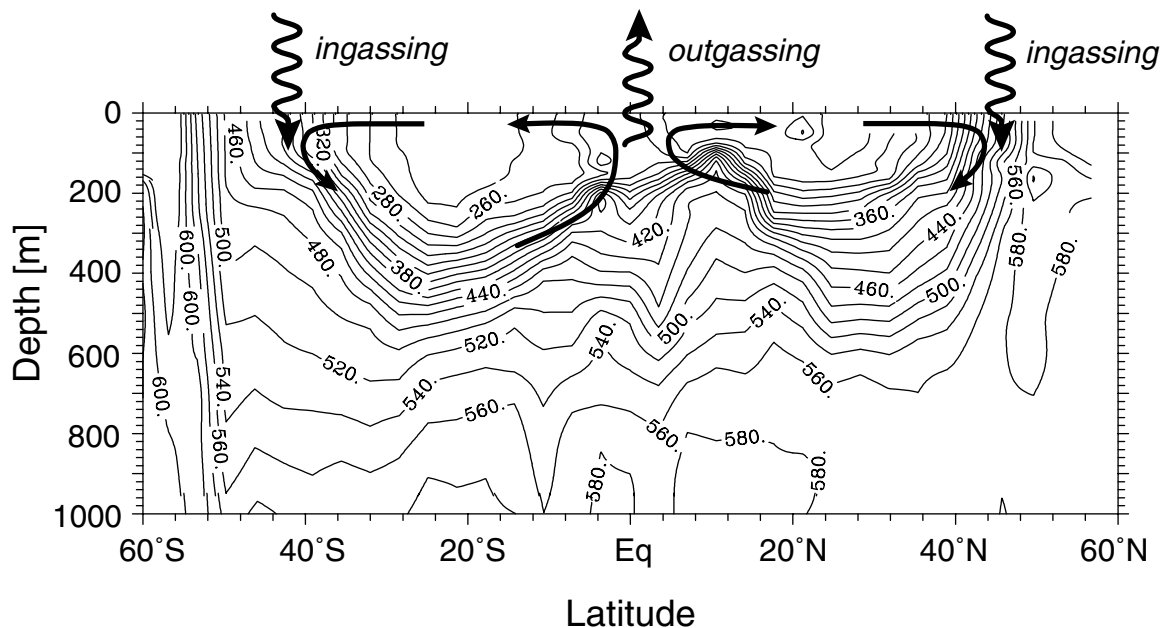


Figure 2. Illustration of the O_2^* inversion concept using data from a meridional section in the central Pacific along WOCE line P16 ($\sim 150^\circ$ W). Upwelling near the equator brings water with elevated O_2^* concentration to the surface, where O_2 is lost to the atmosphere, resulting in a drop of O_2^* . As the upwelled water is transported poleward by the Ekman drift, it starts to take up O_2 again from the atmosphere poleward of $\sim 25^\circ$. By the time surface waters reach the subtropical convergence zone, O_2^* concentrations are nearly back to the values exhibited by the waters feeding the equatorial upwelling.

As the first step in this inversion scheme the surface of the ocean is divided into n regions. Temporally constant fluxes φ_i of n dye tracers are then released from these regions at the ocean surface in an OGCM that is then integrated forward in time until the spatial patterns of these dyes approach a “quasi”-stationary state. The simulated concentration pattern at this time is then sampled at the observation stations and arranged in a column vector \vec{c}_i . In the last step these vectors are combined linearly, such that they differ minimally from the observed concentrations, \vec{c}_{obs} . We thus minimize the expression,

$$\left| \vec{c}_{\text{obs}} - \sum_{i=1}^n \lambda_i \vec{c}_i \right|^2, \quad (2)$$

where λ_i are multipliers. The estimate of the flux of region i itself is then $\lambda_i \varphi_i$.

In practice, (2) is minimized by singular value decomposition [Press *et al.*, 1992]. To do so, the vectors \vec{c}_i are combined to form the matrix $\mathbf{A} = (\vec{c}_1, \vec{c}_2, \dots, \vec{c}_n)$. This matrix is composed of numbers that relate the surface fluxes to their corresponding impact on ocean concentrations. The resulting concentration predicted by the fluxes is thus $\vec{c} = \mathbf{A} \vec{\lambda}$. The modeled distributions, \vec{c}_i^* at the observation stations are replaced with the observed ones, \vec{c}_{obs} , and the solution of the minimization problem is given by the product of the “pseudoinverse” of \mathbf{A} with the observations \vec{c}_{obs} , i.e., $\vec{\lambda} = \mathbf{A}^{-1} \vec{c}_{\text{obs}}$ and fluxes $\vec{F} = \vec{\lambda} \vec{\varphi}$. For further details, particularly with regard to the possible addition of a priori information, the reader is referred to Gloor *et al.* [this issue].

Before we go on and describe the specific application of the inversion scheme used in this study, it is necessary to clearly summarize the assumptions made. The primary assumption of this inversion method is that the employed OGCM accurately reproduces the real ocean circulation. While the uncertainties introduced by this assumption are not captured by the error analysis of the

method itself [see Gloor *et al.*, this issue], the sensitivity of the inversion results to this assumption can be investigated by using several OGCMs that encompass a range of possible model solutions. The sensitivity studies analyzed by Gloor *et al.* [this issue] showed, in the case of heat fluxes, that the inversion results are, indeed, quite sensitive to this assumption, suggesting that great care must be taken in interpreting the results. The results of similar sensitivity studies for oxygen will be discussed below.

This inversion method also implicitly assumes that the ocean circulation and the oxygen cycle are at steady state, neglecting any temporal variations on interannual and longer timescales. This assumption is largely based on the observation that the atmospheric CO_2 concentration has varied by <10 ppm over the last 4000 years before the onset of the industrial revolution [Indermühle *et al.*, 1999; Etheridge *et al.*, 1996]. This requires that sources and sinks of carbon must have been very nearly balanced since the residence time of CO_2 in the atmosphere is a few years only. Because the cycling of oxygen is very tightly linked with that of CO_2 , this requires also that the sources and sinks of oxygen must have been in close balance in preindustrial times. The burning of fossil fuels and land use change have led to a perturbation of the CO_2 and oxygen cycles. However, the resulting decrease of O_2 in the atmosphere is miniscule ($<0.1\%$) relative to the total amount of oxygen in the atmosphere, and therefore it can be neglected for the purpose of this calculation.

In the specific application of this oceanic inversion to estimate net air-sea fluxes of O_2 we make the additional assumption that the stoichiometric oxygen-to-phosphate ratio $r_{O_2:PO_4}$ is constant and has a value of -170 . The validity of this assumption has been the subject of intense debate [Takahashi *et al.*, 1985; Minster and Boulahtid, 1987; Boulahtid and Minster, 1989; Anderson and Sarmiento, 1994; Shaffer *et al.*, 1999; Pahlow and Riebesell, 2000] ever since the existence of relatively constant stoichiometric ratios for oceanic photosynthesis and respiration was suggested by Redfield *et al.* [1963]. There are many reasons to believe that $r_{O_2:PO_4}$

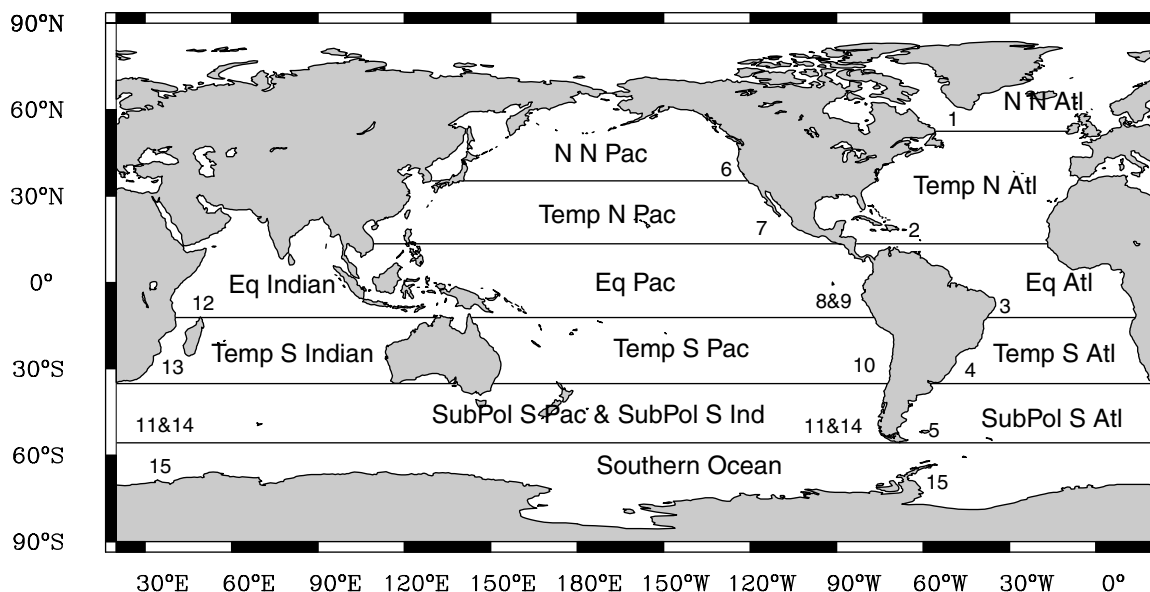


Figure 3. Map showing the 13 regions used for the oceanic inversion. The boundaries are at 58°S, 36°S, 13°S, 13°N, and 36°N in the Pacific and 53°N in the Atlantic. The Arctic Ocean has been combined with the polar North Atlantic.

should be variable since the remineralization of PO_4 is not tightly linked to the consumption of O_2 . However, the most thorough investigation to date by *Anderson and Sarmiento* [1994] shows that below 400 m, the remineralization of organic matter can be described by constant remineralization ratios with a value for $r_{\text{O}_2:\text{PO}_4}$ of $-170 \pm 10:1$. At present, no global examinations of stoichiometric ratios above 400 m exist, but one can expect higher variability in the ratios as one approaches the euphotic zone. Elevated C:P ratios (which imply elevated $r_{\text{O}_2:\text{PO}_4}$) have been reported, for example, from the subtropical North Pacific [*Karl et al.*, 1997; *Abell et al.*, 2000], but the extent to which these observations apply are presently not known. Our assumption of a constant $r_{\text{O}_2:\text{PO}_4}$ ratio therefore has to be regarded as a working hypothesis. Since we do not take possible variations of $r_{\text{O}_2:\text{PO}_4}$ into account, these variations would show up as variation in O_2^* and would be incorrectly interpreted as the result of air-sea gas exchange. We believe, however, that the influence of a possibly varying $r_{\text{O}_2:\text{PO}_4}$ ratio on our results is relatively small. If the variation of $r_{\text{O}_2:\text{PO}_4}$ are within the reported uncertainty by *Anderson and Sarmiento* [1994] of ± 10 , O_2^* would vary maximally between 0 and $22 \mu\text{mol kg}^{-1}$ depending on the PO_4 concentration. This is between 0 and 4% of the concentration range of O_2^* . We show below that the uncertainty that arises from $r_{\text{O}_2:\text{PO}_4}$ has, indeed, a small impact on the inverse estimates of air-sea gas exchange.

We have neglected so far the influence of N_2 fixation and denitrification on O_2^* , two processes that decouple the stoichiometric link between O_2 and PO_4 . We especially need to worry about denitrification since it produces PO_4 without changing O_2 . However, an analysis of N^* [*Gruber and Sarmiento*, 1997], a tracer reflecting N_2 fixation and denitrification, shows that the contribution of these two processes to variations in O_2^* is relatively small. The tracer N^* varies over most of the ocean by less than $\pm 3 \mu\text{mol kg}^{-1}$, which is $< 5 \mu\text{mol kg}^{-1}$ in O_2^* if an $r_{\text{N:P}}$ ratio of -104 for denitrification and an $r_{\text{N:P}}$ of 125 for N_2 fixation are adopted. In addition, N_2 fixation and denitrification tend to be localized [*Gruber and Sarmiento*, 1997], with the major denitrification sites located in the Arabian Sea and in the eastern tropical Pacific. We can therefore neglect the influence of N_2 fixation and denitrification on O_2^* in most of the world oceans but need to consider their influence in the Arabian Sea and eastern tropical Pacific.

3.1. Regions and Emission Patterns

To set up such an inversion, a choice has to be made of how many regions to consider and which emission patterns to use for the forward predictions. On the basis of the results of *Gloor et al.* [this issue] we partition the ocean surface into 13 regions, guided by the main hydrographic regions of the surface oceans (see Figure 3).

In order to produce optimal results the spatial structure of the emission patterns should closely resemble the pattern of the fluxes to be estimated. This is because the oceanic distribution of O_2^* not only contains information about the strength of the net air-sea fluxes in each region but also about the spatial distribution of these fluxes within each region. While we solve for the first information explicitly, we need to make an a priori assumption for the latter (see *Gloor et al.* [this issue] for further details). However, no reliable estimate of the annual net oxygen flux pattern exists. We therefore use instead an emission pattern modeled after the annual net heat fluxes of *Esbensen and Kushnir* [1981] as employed by *Gloor et al.* [this issue]. This choice is based on our observation above that O_2^* and θ are highly correlated (see Figure 1). It therefore appears reasonable to expect a high correlation between annual net fluxes of oxygen and heat as well. We use a spatially uniform emission pattern as a reference to study the sensitivity of the results to the chosen emission pattern.

3.2. Ocean General Circulation Model

To calculate the transport matrix \mathbf{A} (see section 3), we use three different variants of a 3-D OGCM. The details of these models are described by *Gloor et al.* [this issue].

Our standard model consists of a seasonal 3-D ocean circulation model newly developed at Princeton University on the basis of the Geophysical Fluid Dynamics Laboratory (GFDL) Modular Ocean Model (MOM) version 3 [*Pacanowski and Griffies*, 1998]. We will refer to this model as KVLOW + AILOW [*Gnanadesikan et al.*, 2001]. It is a global model with 24 vertical layers, a zonal resolution of 4.5° and a meridional resolution of $\sim 4^\circ$. Its most prominent features relative to earlier models of the Princeton group are the specification of low explicit vertical mixing, the inclusion of lateral advective trans-

Table 1. Summary of Cruises^a

Cruise ^b	Dates	Ship, Country	Remarks	Reference
<i>Atlantic Ocean</i>				
GE AT	Aug. 1972 to March 1973	Knorr, USA	GEOSECS	Bainbridge [1981]
TTO N	April to Oct. 1981	Knorr, USA	TTO North Atl. Study	PCODF [1986a]
TTO T	Dec. 1982 to Feb. 1983	Knorr, USA	TTO Tropical Atl. Study	PCODF [1986b]
HUD82	Feb. to April 1982	Hudson, CAN	winter cruise	PCODF [1984]
SAVE2	Nov. 1987 to April 1989	Knorr, USA	SAVE	ODF [1992a, 1992b]
AJAX2	Oct. 1983 to Feb. 1984	Knorr, USA	AJAX Long Lines	PCODF [1985]
OC133	May 1983	Oceanus, USA	cruise 133	WHPO [1996a]
OC134	June to July 1983	Oceanus, USA	cruise 134	
AT109	June to July 1981	Atlantis II, USA	cruise 109	Roemmich and Wunsch [1985]
HE [1906]	July to Aug. 1992	Hesperides, SP	WOCE cruise A05	Parrilla et al. [1994]
OC202	July to Aug. 1988	Oceanus, USA	cruise 202, WOCE A16N	WHPO [1996b]
ME115	Jan. to March 1990	Meteor, GER	WOCE cruises S1/2 and A21/22	Chipman et al. [1994]
ME153	Feb. to March 1991	Meteor, GER	WOCE cruise A09	Johnson et al. [1995]
ME181	Sept. 91	Meteor, GER	WOCE cruise A01E	Johnson et al. [1996]
DI199	Dec. 1992 to Jan. 1993	Discovery, USA	WOCE cruise A11	
ANT_V	June 1986 to Dec. 1986	Polarstern, GER	ANT. Winter Weddell Sea Exp.	
ANT_8	Sept. to Nov. 1989	Polarstern, GER	ANT. VIII/2 and VIII/3	Augstein et al. [1991]
ANT10	May to July 1992	Polarstern, GER	ANT. X/4 (WOCE A12)	
ANT10	Dec. 1992 to Jan. 1993	Polarstern, GER	ANT. X/7 (summer)	
SAT91	July to Aug. 1991	M. Baldrige, USA	NOAA/AOML South Atl. 1991	Forde et al. [1994]
NAT93	July to Aug. 1993	M. Baldrige, USA	NOAA/AOML North Atl. 1993	
<i>Pacific Ocean</i>				
GE PA	Aug. 1973 to May 1974	Melville, USA	GEOSECS	Broecker et al. [1982]
TP24	March 1983 to June 1985	T. Thompson, USA	WOCE cruise P3	Swift et al. [1990]
TP47	Aug. 85 to Sept. 1985	T. Thompson, USA	WOCE cruise P1	Talley et al. [1988]
MW893	Feb. to May 1989	Maona Wave, USA	WOCE cruise P4	
TUNE1	May to July 1991	T. Washington, USA	WOCE cruise P17C	Goyet et al. [1997]
TUNE2	July to Aug. 1991	T. Washington, USA	WOCE cruises P16S, P17S	Takahashi et al. [1996]
TUNE3	Aug. to Oct. 1991	T. Washington, USA	WOCE cruise P16C	Goyet et al. [1996]
K138W	May to July 1992	Knorr, USA	WOCE cruise P6	
K138W	Oct. to Nov. 1992	Knorr, USA	WOCE cruise P16A/P17A	Rubin et al. [1998]
K138W	Dec. 1992 to Jan. 1993	Knorr, USA	WOCE cruise P17E/P19S	Rubin et al. [1998]
K138W	Feb. to April 1993	Knorr, USA	WOCE cruise P19C	Rubin et al. [1998]
CGC90	Feb. to April 1990	M. Baldrige, USA	NOAA/PMEL CGC-90	Lamb et al. [1995]
CGC92	Aug. to Oct. 1992	Vickers, USA	NOAA/PMEL CGC-92	
CGC94	Jan. to April 1994	M. Baldrige, USA	NOAA/PMEL CGC-94 (P18)	
EQPAC	Feb. to May 1992	M. Baldrige, USA	NOAA/PMEL Eq. Pacific spring	
EQPAC	Sept. to Dec. 1992	M. Baldrige, USA	NOAA/PMEL Eq. Pacific fall	
AK_IO	Feb. to April 1992	Akademik Ioffe, RU	WOCE cruise S4P	Chipman et al. [1997]
<i>Indian Ocean</i>				
GE_IN	Dec. 1977 to April 1978	Melville, USA	GEOSECS	Weiss et al. [1983]
INDGO	Feb. 1985 to Feb. 1987	M. Dufresne, FR	INDIGO	
CIVA1	Feb. to March 1993	M. Dufresne, FR	WOCE cruise I06S	
I1	Aug. to Oct. 1995	Knorr, USA	Knorr 145-11, WOCE I1	WHPO [2000]
I2	Dec. 1995 to Jan. 1996	Knorr, USA	Knorr 145-11, WOCE I2	WHPO [2000]
I3	April to June 1995	Knorr, USA	Knorr 145-8, WOCE I3	WHPO [2000]
I5W14	June to July 1995	Knorr, USA	Knorr 145-9, WOCE I5W14	WHPO [2000]
I7N	July to Aug. 1995	Knorr, USA	Knorr 145-10, WOCE I7N	WHPO [2000]
I8NI5E	March to April 1995	Knorr, USA	Knorr 145-7, WOCE I8NI5E	WHPO [2000]
I8SI9S	Dec. 1994 to Jan. 1995	Knorr, USA	Knorr 145-5, WOCE I8SI9S	WHPO [2000]
I9N	Jan. to March 1995	Knorr, USA	Knorr 145-6, WOCE I9N	WHPO [2000]
I10	Nov. 1995	Knorr, USA	Knorr 145-13, WOCE I10	WHPO [2000]
S4I	May to July 1996	Palmer, USA	WOCE S4I	WHPO [2000]
DA29	Nov. to Dec. 1987	C. Darwin, USA	WOCE I05P	WHPO [2000]

^aCAN, Canada; SP, Spain; GER, Germany; RU, Russia; FR, France; GEOSECS, Geochemical Ocean Sections Study; TTO, Transient Tracers in the Oceans; Atl., Atlantic; SAVE, South Atlantic Ventilation Experiment; WOCE, World Ocean Circulation Experiment; ANT, Antarctic; Exp., Experiment; NOAA, National Oceanic and Atmospheric Administration; AOML, Atlantic Oceanographic and Meteorological Laboratory; PMEL, Pacific Marine Environmental Laboratory; Eq., equatorial; PCODF, Physical and Chemical Oceanographic Data Facility; ODF, Oceanographic Facility; WHPO, WOCE Hydrographic Programme Office.

^bCruise/program descriptor

port by eddies following the parameterization of Gent et al. [1995], and the opening of the Arctic to permit net flow from the North Pacific through the Bering Strait into the North Atlantic [Gnanadesikan et al., 2001]. The use of the Gent–McWilliams parameterization [Gent et al., 1995] led to a strong flattening of isopycnal surfaces in the Southern Ocean and an almost complete shutdown of convection. This resulted in a very sluggish ventilation of the deep ocean from Southern Hemi-

sphere sources. Simulations of radiocarbon and chlorofluorocarbon reveal that this shutdown is likely too strong [Dutay et al., 2001]. In order to investigate the effect of this very small deep water production in the Southern Ocean on the inversion results we also use a model whose vertical diffusivity in the Southern Ocean south of 50°S was increased about sixfold to reduce the excessive stratification. This model will be referred to as KVHISOUTH + AILOW [Gnanadesikan et al., 2001].

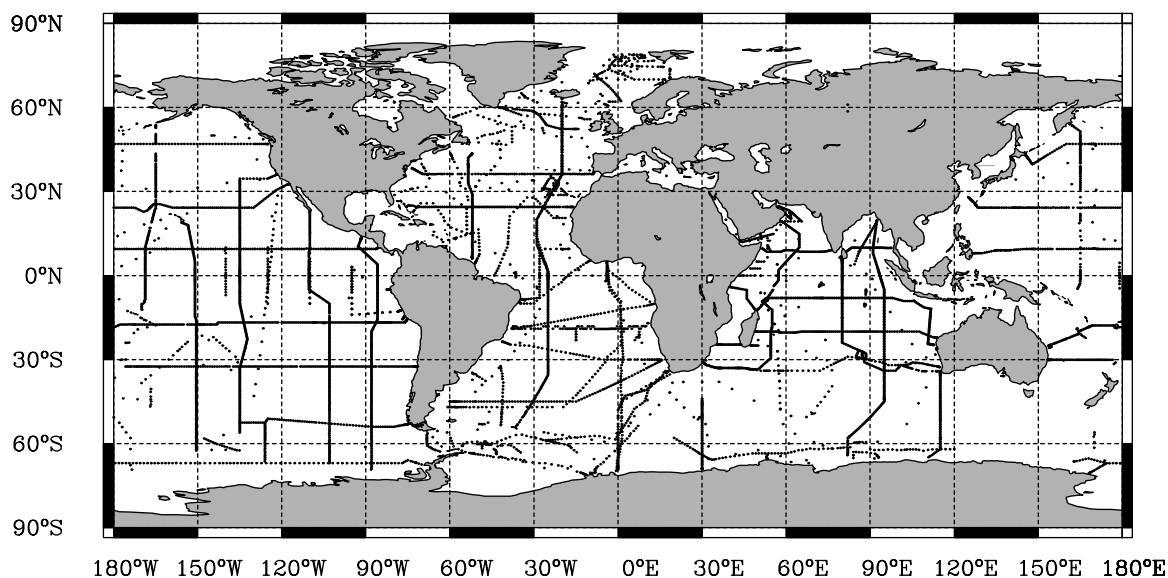


Figure 4. Map showing the station locations of the cruises used in this study. See Table 1 for cruise details.

The third ocean circulation model is the SIL model developed by *Gnanadesikan* [1999] to study the cycling of silicon in the ocean. This model has many similarities to KVLOW + AILOW in that it has the same horizontal resolution, it uses low explicit vertical diffusivity, and it includes the lateral advective effect of eddies by employing the Gent–McWilliams parameterization. The main differences are that it has only 12 layers vertically, that its topography neither allows for flow through the Bering Strait nor through the Indonesian Straits, and that it is an annual mean model.

After spinning up the OGCMs for 4000 years, the dye emissions were turned on, and the models integrated for an additional 3000 years, until the spatial distribution of the dyes reached a quasi-stationary state. At this point in time, the concentration of the dyes is increasing at the same rate everywhere, but the structure of the dye distributions remains the same. All inversions were done using annual mean results from model year 7000.

3.3. Data

In order to produce a high-quality data set of temperature, phosphate, and oxygen with global coverage we assembled hydrographic data from >50 cruises into a homogeneous data set. The cruises are listed in Table 1, and the station locations are shown in Figure 4. In total the database consists of ~5000 stations with >180,000 observations and provides good spatial coverage of all basins. Internal consistency of the different data sets is crucial since we are looking at small deviations in the oxygen and phosphate fields, particularly in the deep ocean. We investigated the internal consistency by examining deep ocean trends at crossover stations or closely revisited regions. This analysis revealed several systematic offsets, mainly in phosphate, that we interpreted as being caused by systematic differences in sampling and analysis. We therefore applied various corrections to the phosphate data as summarized by *Gruber and Sarmiento* [1997] for the Atlantic and by *Deutsch et al.* [2001] for the Pacific. Most of these PO₄ corrections, however, were <0.05 μmol kg⁻¹, which is equivalent to ~9 μmol kg⁻¹ in O₂^{*}. The cruises span a period of >20 years (1972–1995). Although changes in water mass properties and circulation patterns have been reported for this period in various regions [e.g., *Brewer et al.*, 1983; *Levitus*, 1989a, 1989b; *Graham*, 1994; *White and Peterson*, 1996], we do not take them into account and combine

the data as if they were synoptic because, first, excluding data from regions where changes have been reported would reduce our data coverage and, second, we expect the influence of these physical variations on our inversion results to be very small since the reported temperature changes are generally relatively small (most are <0.2°C, which is equivalent to a change of ~0.8 μmol kg⁻¹ in the oxygen saturation concentration).

Gloor et al. [this issue] analyzed the quality of this network with respect to estimating heat fluxes. They found little difference in inversely estimated heat fluxes and concluded from this that our network is sufficient for constraining the inversion.

4. Results and Discussion

4.1. Air-Sea Oxygen Fluxes

Figure 5 shows the inversely estimated annual net oxygen fluxes across the air-sea interface for the standard model (KVLOW(h), see Table 2). The 13 considered regions have been arranged from south to north to emphasize global meridional trends. Integrated fluxes are tabulated in Table 3 for two cases. In the first case the global inversion was computed without any additional constraint, whereas in the second case a global balance constraint was added, i.e., the global net air-sea flux of O₂ was forced to be zero. In the unconstrained case the regionally integrated oxygen fluxes add up to a loss of 49 Tmol O₂ yr⁻¹ globally. This is a relatively small imbalance, given the observation that the corresponding global mean aerial flux of 0.14 mol O₂ m⁻² yr⁻¹ is <10% of the mean absolute flux estimated for the 13 regions. It is interesting to note that the magnitude of this imbalance is very similar to estimates of current O₂ outgassing caused by the warming of the ocean [*Plattner et al.*, 2001]. Adding a balance constraint changes the results only slightly, with the exception of the northern North Atlantic and the regions south of 36°S. It is thus encouraging to note that our inversion is not overly sensitive to this constraint.

The uncertainties of these flux estimates determined by error propagation (see equation (5) of *Gloor et al.* [this issue]) are very small. This is because a large number of observations (180,000) are used to estimate only 13 parameters. We therefore did not add these uncertainties to the estimates listed in Table 3. It is important to point out that while the statistical uncertainties are small, systematic errors (biases) are large and determine the overall uncertainties

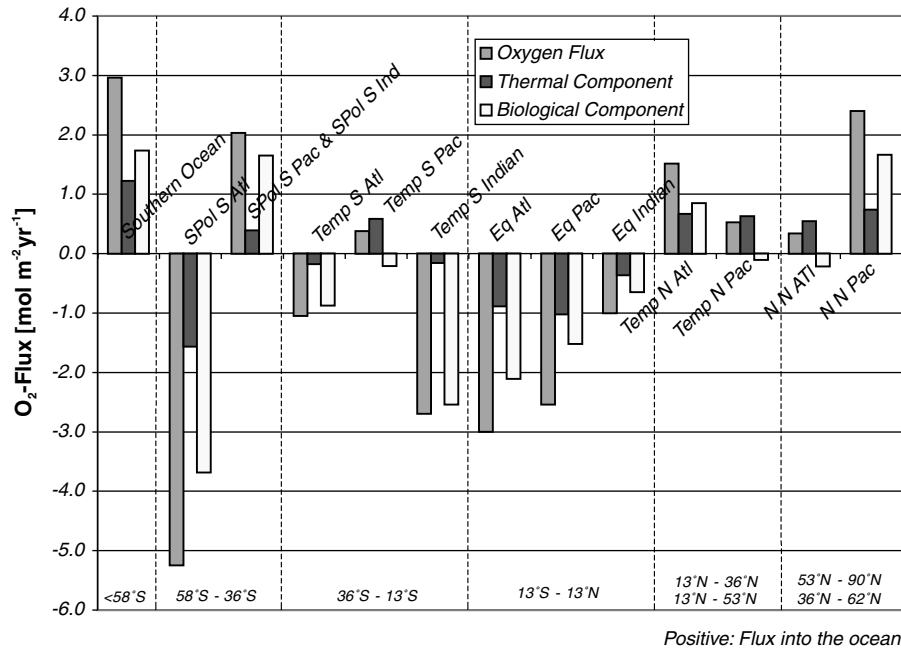


Figure 5. Plot of the inversely estimated oxygen fluxes for 13 regions using observed O_2^s data. Shown are the mean fluxes of the different regions. These inversion results are based on our standard OGCM (KVLOW + AILOW) with the emission pattern structured spatially after the net heat fluxes of *Esbensen and Kushnir* [1981]. The results are arranged in six zonal bands, with the southernmost band plotted on the left side. Positive numbers indicate oxygen uptake by the ocean. Also shown is the separation of the estimated oxygen fluxes into a thermal and biological component using the inversely estimated net heat fluxes (see text for details).

in our inversion problem. We make an attempt to assess the biases by sensitivity studies discussed below.

The main pattern that emerges from Figure 5 is uptake of oxygen in the high latitudes of both hemispheres and release of oxygen into the atmosphere in the low latitudes. This pattern is as expected from the temperature sensitivity of oxygen and the distribution of O_2^s (see Figure 1). The general cooling of waters in high latitudes increases the solubility of oxygen in the surface waters, thereby promoting a flux of oxygen into the ocean from the atmosphere. At the same time, incomplete utilization of nutrients in the surface waters in these regions leads to a net “biological” demand of oxygen from the atmosphere since the oxygen undersaturation that is transported and mixed to the surface from below is not fully compensated by the biological oxygen production. Hence cooling and incomplete biological utilization act together to create a net flux of oxygen from the atmosphere into the ocean in the high latitudes.

These two processes are operating in opposite direction in the low latitudes. Warming of the waters decreases the solubility of

oxygen, thereby driving oxygen out of the surface waters. At the same time, any nutrient that is brought to the surface is usually completely utilized, leading to an excess of biological oxygen production over the oxygen demand stemming from the nutrient-associated transport of undersaturated waters. Hence it appears that over most of the ocean, ocean biology and heat fluxes tend to reinforce each other in creating the oxygen fluxes.

We can investigate this in more detail by separating the oxygen flux F_{O_2} into a component driven by heat fluxes (“thermal component”, $F_{O_2}^{\text{therm}}$) and a component driven by biological production and demand (“biological component”, $F_{O_2}^{\text{bio}}$), thus

$$F_{O_2} = F_{O_2}^{\text{bio}} + F_{O_2}^{\text{therm}}. \quad (3)$$

Since the air-sea gas exchange of oxygen is relatively rapid (reequilibration of O_2 in a mixed layer of 50 m occurs on timescales of days), which allows surface ocean O_2 to respond quickly to the net exchange of heat across the air-sea interface, the

Table 2. Summary of Sensitivity Studies

Study	OGCM	Emission Pattern ^a	$r_{O_2:PO_4}$
Standard (KVLOW(h))	KVLOW + AILOW ^b	heat	−170
KVLOW(u)	KVLOW + AILOW	uniform	−170
KVHISOUTH(h)	KVHISOUTH + AILOW ^c	heat	−170
SIL(u)	SIL ^d	uniform	−170
KVLOW(rop − 10)	KVLOW + AILOW	heat	−180
KVLOW(rop + 10)	KVLOW + AILOW	heat	−160

^a Heat, emission pattern based on heat fluxes of *Esbensen and Kushnir* [1981]; uniform, spatially uniform emission pattern.

^b Standard model as explained in section 3.2 [*Gnanadesikan et al.*, 2001].

^c As KVLOW + AILOW, except that vertical diffusivity in the Southern Ocean south of 60°S has been increased to $10^{-4} \text{ m}^2 \text{ s}^{-1}$ [*Gnanadesikan et al.*, 2001].

^d OGCM employed by *Gnanadesikan et al.* [1999] to study the oceanic cycling of silicon.

Table 3. Regionally Integrated O₂ Fluxes Estimated by Standard Case of Inversion (KVLOW(h))^a

Region	Area, 10 ¹³ m ²	Unconstrained			Balance Constraint ^c		
		$\int F_{O_2} dA$ Tmol yr ⁻¹	$\int F_{O_2}^{therm} dA^b$ Tmol yr ⁻¹	$\int F_{O_2}^{bio} dA^b$ Tmol yr ⁻¹	$\int F_{O_2} dA$ Tmol yr ⁻¹	$\int F_{O_2}^{therm} dA^b$ Tmol yr ⁻¹	$\int F_{O_2}^{bio} dA^b$ Tmol yr ⁻¹
<i>Atlantic</i>							
Northern North Atlantic	1.912	6.4	10.4	-4.0	9.4	8.8	0.6
Temperate North Atlantic	3.073	46.5	20.5	26.1	65.7	18.8	46.9
Equatorial Atlantic	1.675	-50.1	-14.8	-35.3	-56.7	-17.5	-39.2
Temperate South Atlantic	1.484	-15.5	-2.6	-12.9	-10.8	-3.9	-6.9
<i>Pacific</i>							
N. North Pacific	1.892	45.4	14.0	31.4	52.0	12.9	39.1
Temperate North Pacific	3.374	17.6	21.1	-3.5	20.5	17.3	3.2
Equatorial Pacific	4.963	-125.8	-50.5	-75.3	-128.2	-56.9	-71.3
Temperate South Pacific	3.435	13.0	20.0	-7.0	20.0	16.6	3.5
<i>Indian</i>							
Equatorial Indian	2.781	-27.9	-10.0	-17.8	-27.5	-13.4	-14.1
Temperate south Indian	2.044	-55.0	-3.2	-51.8	-52.5	-5.5	-47.1
<i>Southern Ocean</i>							
Subpolar South Atlantic	1.563	-82.0	-24.4	-57.6	-103.1	-30.5	-72.6
Subpolar South Pacific and Subpolar south Indian	5.027	102.2	19.4	82.7	74.5	9.2	65.2
Southern Ocean	2.588	76.6	31.7	44.9	136.8	44.1	92.7
<i>Integrated Fluxes</i>							
Global	35.811	-48.7	31.5	-80.2	0.0	0.0	0.0
South of 13° S	16.141	39.2	40.9	-1.7	64.8	30.0	34.8
North of 13° N	10.250	116.0	66.0	49.9	147.6	57.8	89.8
Tropics	9.419	-203.9	-75.4	-128.5	-212.4	-87.8	-124.6

^a Fluxes are positive for net uptake of oxygen by the ocean.

^b Separation of $\int F_{O_2} dA$ into a thermal component ($\int F_{O_2}^{therm} dA$) and biological component ($\int F_{O_2}^{bio} dA$) was computed on the basis of (3) and (4) using the inversely estimated heat fluxes of Gloor *et al.* [this issue].

^c A global balance constraint has been added for the oxygen inversion to ensure that the global integrated flux sums to zero. This does not ensure, however, that the thermal and biological components balance individually since the temperature derivative of the oxygen saturation concentration is strongly temperature dependent and therefore varies from region to region. These two fluxes therefore have been adjusted uniformly on a global basis. For $\int F_{O_2}^{therm} dA$ and $\int F_{O_2}^{bio} dA$ the adjustments were 0.12 mol m⁻² yr⁻¹ and -0.12 mol m⁻² yr⁻¹, respectively.

thermal component $F_{O_2}^{therm}$ can be estimated from the net exchange of heat Q and the temperature dependence of the oxygen solubility $\partial[O_2^{sat}]/\partial T$ [Keeling and Peng, 1995]:

$$F_{O_2}^{therm} = \frac{Q}{c_p} \frac{\partial[O_2^{sat}]}{\partial T}, \quad (4)$$

where c_p is the heat capacity of seawater computed according to Millero *et al.* [1973]. For Q we use the inversely estimated heat fluxes of Gloor *et al.* [this issue]. These heat flux estimates were obtained in an identical manner to our oxygen fluxes by inverting the observed temperature data. The temperature dependence of the oxygen solubility was computed from the oxygen solubility formulation reported by Weiss [1970]. The separation of the net oxygen flux into a thermal and biological component is not without caveats. The net exchange of heat across the air-sea interface is the sum of many distinct individual processes (i.e., sensible heat, latent heat, and shortwave radiation), while the air-sea exchange of oxygen is a single process driven by the gradient of the oxygen partial pressure across the air-sea interface. Therefore only the observation that O₂ in the surface ocean reequilibrates within a few days after a net heat flux has altered the temperature and hence the solubility permits us to separate the oxygen fluxes into a thermal and biological component. It is interesting to note that this separation is not possible for CO₂ since this gas has a much longer equilibration timescale [Broecker and Peng, 1974].

The thermal and biological components of the oxygen fluxes calculated by applying (3) and (4) to the inversely estimated oxygen and heat fluxes are consistent with the hypothesis that the thermal and biological components usually act in the same direction and thus tend to reinforce each other (Figure 5). Figure 5 also shows that on average, the biological component dominates over

the thermal component, particularly when the oxygen fluxes are large. These findings are in good agreement with our analysis of the O₂* data in Figure 1. In three regions (temperate South Pacific, temperate North Pacific, and northern North Atlantic) the thermal component of the oxygen flux dominates and acts in opposite direction of the biological flux. The fluxes in these regions are small, however, and hence have little impact on the overall trend.

Closer inspection of the inversion results reveals that the overall pattern of oxygen release in the low latitudes and uptake in the high latitudes does not apply in the subpolar South Atlantic (58°–36°S). According to our inversion, this region is a substantial source of oxygen to the atmosphere, whereas the subpolar region in the Indo-Pacific represents a sink for the atmosphere in accordance with the large-scale pattern. This difference between the Atlantic and Indo-Pacific is possibly a consequence of the global thermohaline circulation. In the subpolar South Atlantic, surface and upper thermocline waters flow northward to compensate the export of North Atlantic Deep Water in the deep layers. Along their pathway northward these upper ocean waters are being warmed and lose nutrients owing to biological uptake. Both these processes lead to a strong outgassing of oxygen from the ocean. Since no deep waters are formed in the North Pacific and in the northern Indian Ocean, these basins are lacking such an upper ocean net northward transport in their Southern Hemisphere subpolar regions [Ganachaud *et al.*, 2000; Ganachaud and Wunsch, 2000] and hence do not have such outgassing of oxygen in these regions. Another possibly linked explanation for the O₂ flux difference between the subpolar South Atlantic and the subpolar Indo-Pacific might be the observation that the subpolar South Atlantic has higher chlorophyll levels and lower nutrient concentrations on average than the subpolar Indo-Pacific and therefore has much less the characteristics of a High-Nutrient Low-Chlorophyll (HNLC) area.

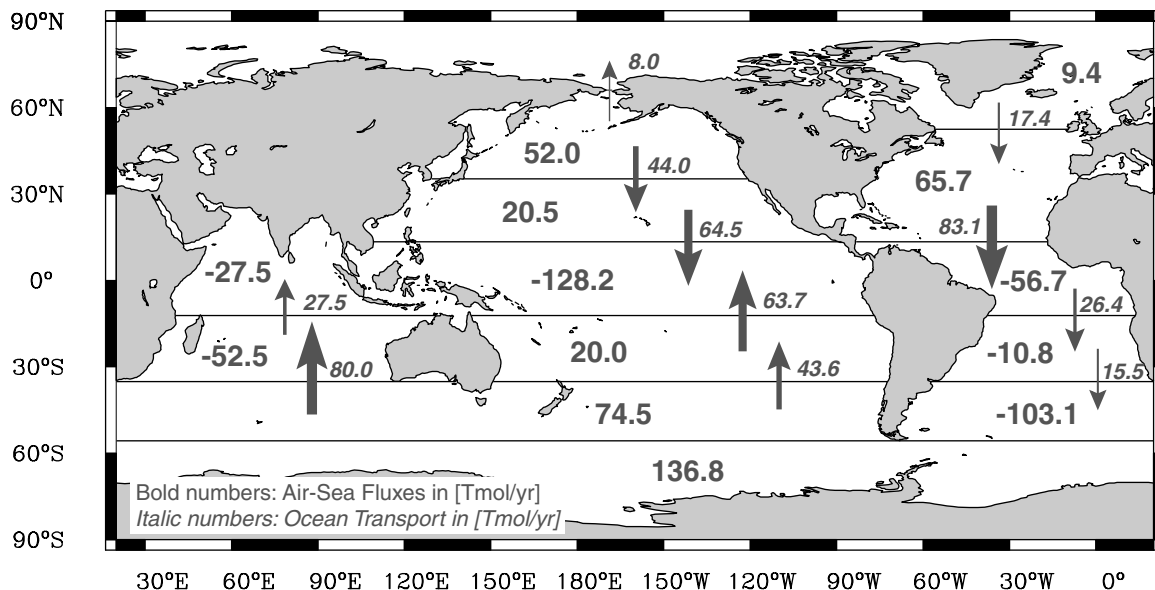


Figure 6. Global map of air-sea fluxes and implied ocean transport of O₂ as estimated from the inversion of O₂^{*}. The ocean transport estimates have been obtained by setting the O₂ transport across the Bering Strait to 8 Tmol yr⁻¹ and then integrating the air-sea fluxes southward. These inversion results are based on our standard OGCM (KVLOW + AILOW) with the emission pattern structured spatially after the net heat fluxes of *Esbensen and Kushnir* [1981] and using a global balance constraint to enforce zero net flux of O₂ across the air-sea interface.

4.2. Ocean Transport of Oxygen

Since we assumed steady state, we can integrate the inversely estimated air-sea oxygen fluxes over the surface regions and compute the implied ocean transport of oxygen. We start the integration at the North Pole and take into account 8 Tmol yr⁻¹ transport of O₂ across the Bering Strait, computed by assuming a mass transport of 0.8 Sv [*Coachman and Aagaard*, 1988] and a mean oxygen concentration of $\sim 320 \mu\text{mol kg}^{-1}$ in the waters of the straits [*Levitus and Boyer*, 1994]. We take this transport through the Bering Strait into account in order to be able to compare our estimates with those based on hydrographic sections, which often include this transport (see *Holfort et al.* [1998] for discussion). The computed ocean transports are shown on a global map in Figure 6 and versus latitude in Figure 7.

The ocean uptake of oxygen from the atmosphere in the entire North Atlantic coupled with the relatively small outgassing in the tropical Atlantic leads to a southward oxygen transport across 13°S in the Atlantic of 26 Tmol O₂ yr⁻¹ (83 Tmol O₂ yr⁻¹ across 13°N). This transport across 13°S in the Atlantic is, however, more than compensated for in the Indo-Pacific, where the strong outgassing computed for the equatorial Pacific and equatorial Indian Ocean requires a strong convergence in the equatorial regions, resulting in the transport of 92 Tmol yr⁻¹ northward across 13°S. On a global scale the inversion results predict that of the $\sim 212 \text{ Tmol O}_2 \text{ yr}^{-1}$ outgassing in the equatorial regions, $\sim 148 \text{ Tmol O}_2 \text{ yr}^{-1}$ are being supplied from the Northern Hemisphere across 13°N and $\sim 65 \text{ Tmol O}_2 \text{ yr}^{-1}$ are being supplied from the Southern Hemisphere across 13°S. This implies a substantial asymmetry of $\sim 83 \text{ Tg O}_2 \text{ yr}^{-1}$ in the oxygen uptake between the two hemispheres poleward of 13°, with the Northern Hemisphere being a stronger sink for atmospheric O₂. The hemispheric asymmetry in oxygen fluxes should lead to a lower atmospheric potential oxygen in the Northern Hemisphere compared with the Southern Hemisphere, qualitatively consistent with the analysis of APO by *Stephens et al.* [1998]. A more quantitative comparison below using an atmos-

pheric tracer transport model will show that our inversion produces an interhemispheric difference in mean APO concentration that is consistent with observations but underestimates the pole to pole difference.

Direct estimates of ocean transport of oxygen based on hydrographic data provide one of the few means to compare our inversely estimated oxygen fluxes with independent estimates. Figure 7 shows oxygen transport estimates in the Atlantic and Indo-Pacific from a number of such studies. Our transport estimates generally compare well with these more direct transport estimates, including the only other study that attempted to estimate oxygen transport estimates in all ocean basins [*Ganachaud*, 1999]. The only difference exists in the southern part of the combined Indo-Pacific basin, where our inversion results indicate a larger northward transport than found by *Ganachaud* [1999]. Such a discrepancy is not unexpected since, as discussed below in more detail, there are several lines of evidence that suggest that our inversion has a tendency to overestimate the equatorial outgassing. However, it is important to note that the discrepancy between the results of the two methods is only marginally significant. In summary, we find that the general pattern and magnitude of our air-sea fluxes are consistent with what is presently known about ocean transport of oxygen based on hydrographic data.

4.3. Sensitivity Studies

Before drawing conclusions from the inversely computed air-sea fluxes and ocean transport of oxygen, it is important to investigate the sensitivity of the results to the various assumptions that underly our inversion method. The two main assumptions are (1) a constant stoichiometric oxygen to phosphate ratio of -170 during photosynthesis and remineralization and (2) that the “true” ocean circulation is well represented by our OGCM. We also need to investigate the sensitivity of our inversion to the chosen emission pattern since atmospheric inversion studies demonstrate that the inversion results can be sensitive to these patterns [*Gloor et al.*, 2000].

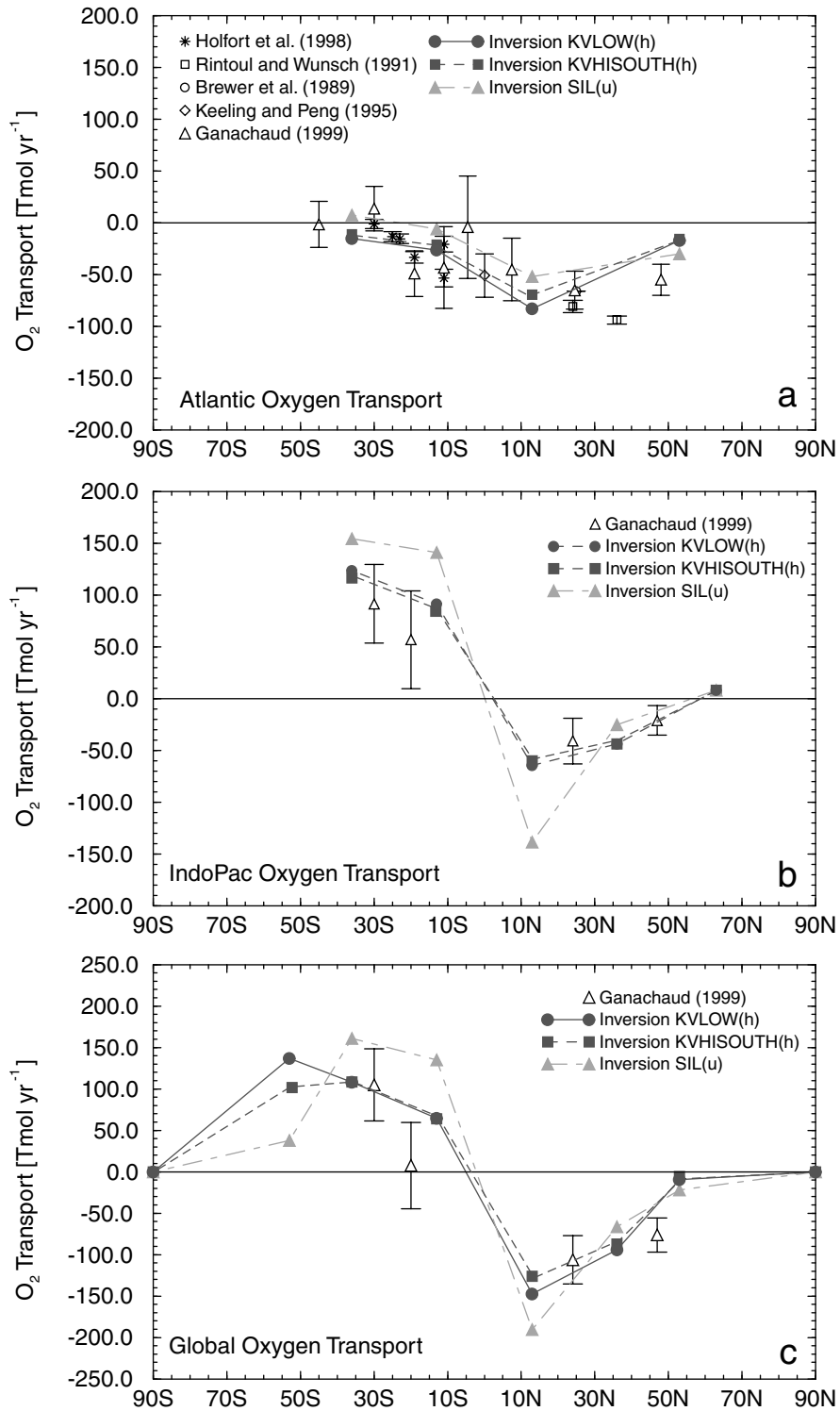


Figure 7. Plots of estimated northward oxygen transports in the ocean versus latitude for (a) the Atlantic Ocean, (b) the combined Indian and Pacific Oceans, and (c) the global ocean. Estimates based on hydrographic transport estimates are shown as symbols with their respective error, while the transport estimates implied by our inversions are shown as lines with symbols. The specifications of the different sensitivity studies are summarized in Table 2.

As it turns out, the inversion results are almost insensitive to variations in the stoichiometric ratio $r_{O_2:PO_4}$ and slightly sensitive to the imposed emission pattern but exhibit considerable sensitivity to the particular OGCM being employed. By changing $r_{O_2:PO_4}$ by

± 10 from its standard value of -170 the estimated O_2 fluxes vary proportionally by only $\sim 6\%$, or a maximum of $8\ Tmol\ yr^{-1}$ (see Table 4). We expect similar proportional changes if $r_{O_2:PO_4}$ was changed spatially nonuniformly. Similar to the small sensitivity to

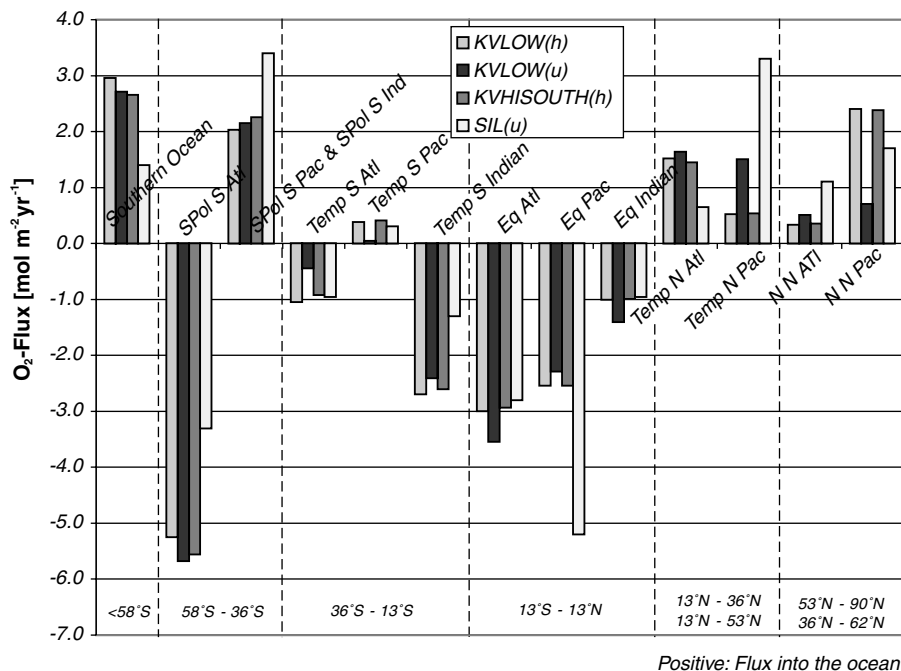


Figure 8. Plot showing the sensitivity of the inversely estimated oxygen fluxes to the structure of the employed emission pattern and to different ocean circulation models. The specifications of the different sensitivity studies are summarized in Table 2.

changes in $r_{\text{O}_2:\text{PO}_4}$, the use of a spatially uniform emission pattern instead of the standard heat emission pattern has relatively little impact on the results with the exception of the northern North Pacific and the temperate North Pacific (see Figure 8 and Table 4). This is because these regions have strong east-west gradients in heat and oxygen fluxes, which are only captured in the spatially structured emission pattern case [Gloor *et al.*, this issue].

In the spatially uniform case (KVLOW(u)) the oxygen release to the atmosphere in the northern North Pacific decreases by $\sim 32 \text{ Tmol yr}^{-1}$ relative to the standard case (KVLOW(h)), whereas the estimated integrated oxygen flux in the temperate North Pacific increases almost by the same amount, keeping the total release of oxygen in the Pacific north of 13°N about the same. The high sensitivity in these two regions to changes in the emission pattern is a consequence of these two regions having very high spatial variability in net heat fluxes [Esbensen and Kushnir, 1981]. In the western North Pacific the northward flowing waters of the Kuroshio lose a large amount of heat to the atmosphere, whereas in the eastern North Pacific, the southward flowing waters in the California Current take up heat from the atmosphere. In contrast, little net heat exchange takes place in the central gyres of the North Pacific. In the regions outside of the North Pacific, the absolute changes in the estimated air-sea fluxes of oxygen are generally $<30\%$, or on average, only 7 Tmol yr^{-1} .

While the inversion results reveal a relatively small sensitivity to changes in the stoichiometric ratio or emission pattern, we find considerable sensitivity of the inversion to changes in the characteristics of the ocean circulation model (see Figure 8 and Table 4). The differences relative to our standard case (KVLOW(h)) are particularly large for the SIL model of Gnanadesikan [1999]. Since the SIL simulations were done with a spatially uniform emission pattern, they are best compared with the KVLOW(u) case. One of the largest differences is seen in the equatorial Pacific, where the SIL(u) estimate is nearly twice as large as that of KVLOW(u). This is likely caused by the SIL model having stronger upwelling and originating from deeper layers in comparison to the KVLOW +

AILOW model. This is a well known deficiency in coarse resolution models [Toggweiler and Samuels, 1993; Toggweiler and Carson, 1995] and was ameliorated in the KVLOW + AILOW model by increasing the vertical resolution by a factor of 2. Analyses of mass budgets and implied export production by Gnanadesikan *et al.* [2001] showed that the KVLOW + AILOW model has an equatorial upwelling that is quite comparable to observational estimates. This is in line with the finding by Gloor *et al.* [this issue] that the inversely estimated heat fluxes by the KVLOW + AILOW model in the tropical regions are of similar magnitude as the observationally based estimates by Esbensen and Kushnir [1981] and da Silva *et al.* [1994], whereas the lower-resolution SIL model estimates unrealistically large heat fluxes.

The stronger outgassing in the equatorial Pacific in SIL(u) is largely compensated by a substantial increase in the oxygen uptake in the North Pacific. The integrated uptake in this region in SIL(u) is more than twice as large as in either KVLOW(h) or KVLOW(u). This difference might be caused by any one or a combination of the following factors: the absence in SIL of flows through the Bering Strait and Indonesian Gap or differences in thermocline ventilation in the North Pacific as a result of lower vertical resolution. We have a better understanding of the lower integrated oxygen uptake in the North Atlantic in the SIL model relative to either the KVLOW + AILOW or KVHISOUTH + AILOW models. The maximum meridional overturning in the Atlantic in the SIL model is only $\sim 12 \text{ Sv}$, whereas the KVLOW + AILOW and KVHISOUTH + AILOW models have a more realistic overturning of $\sim 16 \text{ Sv}$ [Schmitz, 1995]. Since the spatial gradients in O_2^* are fixed by the observations, increasing the water mass transport simulated in the model tends to increase the estimated fluxes in the inversion.

A third area of major differences between SIL(u) and KVLOW(u) is the Southern Ocean and the subpolar South Atlantic, where SIL estimates a lower O_2 uptake in the Southern Ocean but also a lower outgassing in the subpolar South Atlantic. While this change is to some degree caused by differences in the circulation pattern, a significant fraction of these differences might also be due to

Table 4. Results of Unconstrained Sensitivity Cases^a

	Standard	KVLOW(u)	KVHISOUTH(h)	SIL(u)	KVLOW(rop – 10)	KVLOW(rop + 10)
<i>Atlantic</i>						
Northern North Atlantic	6.4	9.6	6.7	21.0	6.0	5.8
Temperate North Atlantic	46.5	50.3	44.4	20.0	43.9	49.4
Equatorial Atlantic	–50.1	–59.3	–49.1	–46.9	–47.3	–53.6
Temperate South Atlantic	–15.5	–6.6	–13.6	–14.1	–14.6	–16.3
<i>Pacific</i>						
Northern North Pacific	45.4	13.2	45.0	32.2	42.8	46.9
Temperate North Pacific	17.6	50.7	17.9	111.3	16.6	20.4
Equatorial Pacific	–125.8	–113.4	–126.0	–258.1	–118.6	–134.4
Temperate South Pacific	13.0	1.5	14.1	10.3	12.3	14.0
<i>Indian</i>						
Equatorial Indian	–27.9	–38.9	–27.5	–26.4	–26.3	–29.0
Temperate South Indian	–55.0	–49.2	–53.1	–26.6	–51.9	–58.0
<i>Southern Ocean</i>						
Subpolar South Atlantic	–82.0	–88.7	–86.8	–51.6	–77.3	–84.3
Subpolar South Pacific and Subpolar South Indian	102.2	107.8	113.2	170.9	96.3	106.9
Southern Ocean	76.6	70.1	68.7	36.2	72.2	76.1
<i>Integrated</i>						
Global	–48.7	–52.7	–46.2	–21.7	–45.9	–56.0
South of 13°S	39.2	34.9	42.4	125.2	36.9	38.4
North of 13°N	116.0	124.0	114.1	184.5	109.3	122.6
Tropics	–203.9	–211.6	–202.7	–331.4	–192.2	–217.0

^a Fluxes are given in Tmol yr^{–1} and are positive for net uptake of oxygen by the ocean. Standard, KVLOW + AILOW model with heat flux pattern; KVLOW(u), KVLOW + AILOW model with uniform flux pattern; KVHISOUTH(h), KVHISOUTH + AILOW model with heat flux pattern; SIL(u), silicate model with uniform flux pattern; KVLOW(rop – 10), standard model with $r_{O_2:PO_4}$ decreased to –180; KVLOW(rop + 10), standard model with $r_{O_2:PO_4}$ increased to –170. See text and Table 2 for further details.

“compensatory” effects caused by a limit in the inversion technique. This problem arises when the signals from two regions are highly correlated, preventing our technique from fully separating the flux in one region from that in another region. This limitation can be investigated by examining the correlation matrix r_{ab} [see Gloor *et al.*, this issue, Figure 3]. As the correlation between the dye signals emitted from the Southern Ocean and the subpolar South Atlantic is higher in SIL(u) than it is in KVLOW(u), it is likely that part of the differences in the inversion results are an artifact of the inversion due to its inability to separate the signals correctly between the two regions.

In contrast to the large changes in the inversion results between KVLOW(u) and SIL(u), increasing the vertical diffusivity in the oceans south of 60°S (KVHISOUTH + AILOW) results in only modest changes in the inversion results. These changes are surprisingly small when considering that the increase in mixing in the Southern Ocean leads to more than a doubling of the CFC inventory in this region [Gnanadesikan *et al.*, 2001]. Therefore, in the case of oxygen, the large uncertainties that are associated with the modeling of the deep and intermediate water formation processes in the Southern Ocean [Orr *et al.*, 2001; Dutay *et al.*, 2001; Caldeira and Duffy, 2000] appear to be of a relatively minor importance.

The impact of the different ocean circulation models on the implied ocean transport of oxygen is shown in Figure 7. Since the estimated fluxes between KVLOW(h) and KVHISOUTH(h) are very similar, the computed oxygen transports are nearly the same. The smaller oxygen uptake estimated by SIL(h) in the North Atlantic leads to a reduced southward transport of oxygen in the Atlantic (Figure 7a). The transport across 13°S amounts only to ~6 Tmol yr^{–1} instead of the 26 Tmol yr^{–1} found for KVLOW(h). Owing to the large differences in air-sea fluxes in the Pacific, the implied oxygen transports for SIL(u) are different in this basin (Figure 7b). The southward transport at 13°N in the Pacific is estimated to be 139 Tmol yr^{–1}, more than twice as large as that found by either KVLOW(h) or KVHISOUTH(h). Because of the large equatorial O₂ loss in the equatorial Indian and equatorial

Pacific the northward flows estimated by SIL(u) in the southern Indo-Pacific are again larger. On the global scale the smaller equatorward transport in the Atlantic and the larger equatorward transport in the Indo-Pacific partially compensate each other, so that the difference between the three models is smaller than the differences found in the individual basins (Figure 7c).

In summary, the inversion results depend to a considerable degree on the ocean circulation model employed. Comparison of the simulated flow pattern, temperature, salinity, natural radio-carbon, and transient tracers with observations indicate that KVLOW + AILOW and KVHISOUTH + AILOW are more successful than SIL [Gnanadesikan *et al.*, 2001; Gnanadesikan, 1999], but these two models still exhibit several shortcomings, most significantly in the Southern Ocean, where tracers indicate that they ventilate too slowly, and the equatorial Pacific, where these coarse-resolution models have a tendency to overestimate the upwelling. However, despite the uncertainties that arise from circulation biases the magnitude and pattern of most estimated oxygen fluxes are rather consistent between all investigated models. The most important exceptions are the Southern Ocean and the equatorial Pacific, where differences of more than a factor of 2 were estimated between the three models investigated.

5. Implications for Atmospheric Potential Oxygen

One of the main conclusions of the study of Stephens *et al.* [1998] was that present ocean biogeochemistry models are deficient in their representation of the interhemispheric transport of carbon and oxygen because their predicted air-sea oxygen and CO₂ fluxes gave atmospheric signals that are incompatible with the observed interhemispheric gradient of APO. The deficiency in the ocean biogeochemistry models with regard to O₂ and CO₂ can stem from any of many possible combinations of errors in ocean transport of mass and heat and from misrepresentation of ocean biogeochemical processes. Since the results from our ocean inver-

sion of O_2^* do not depend on ocean biogeochemistry, we eliminate one of the possible sources of errors.

In order to investigate the APO that results from our inversion we employ an atmospheric tracer transport model and use the annual net oxygen fluxes estimated by the ocean inversion as boundary condition. The model employed is the GFDL global chemical transport model (GCTM) [Mahlman and Moxim, 1978], an off-line atmospheric transport model with a horizontal grid size of ~ 265 km and 11 vertical layers. Since the atmospheric APO signal consists not only of an oceanic O_2 signal but also of a residual fossil fuel signal as well as an oceanic N_2 and CO_2 net flux signal, these tracers needed to be included as well. Furthermore, annual APO variations can also be generated from the seasonal covariance between air-sea fluxes of oxygen, nitrogen, and CO_2 and atmospheric transport and mixing (rectifier effect). The seasonal fossil fuel emissions for the year 1995 were taken from Marland *et al.* [1998], the seasonal net air-sea CO_2 fluxes were based on the climatology of Takahashi *et al.* [1999], and the annual net air-sea fluxes of nitrogen were estimated from the inversely computed annual net heat fluxes using an equation for N_2 analogous to (4). We simulated the seasonal rectifier effect for oxygen and nitrogen on the basis of the seasonal oxygen climatology of Najjar and Keeling [1999] and the seasonal heat flux climatology of Esbensen and Kushnir [1981] after the annual net flux at each grid point was removed.

Figure 9a shows the annual mean simulated APO versus latitude in comparison with the annual mean observed APO at the observation stations reported by Stephens *et al.* [1998] and updated by Stephens [1999] (station locations are shown in Plate 1a). As done by Stephens *et al.* [1998], we shifted the simulated APO to visually fit the mean of the Northern Hemisphere observations. Such an adjustment is justified by the fact that the absolute concentration of APO is arbitrary. The simulated APO distribution at the observation locations agrees fairly well with the observations at most stations. The agreement is generally better in the Northern Hemisphere than that in the Southern Hemisphere. In the Northern Hemisphere the only substantial difference exists at Cold Bay, Alaska (CBA), where the simulated APO is substantially higher than observed. In the Southern Hemisphere the simulated APO is too high at Samoa (SMO) and underpredicts the latitudinal variations between Cape Grim (CGO), Macquarie Island (MCQ), and the South Pole (SPO). The simulations also underpredict the APO concentrations at SPO and CGO relative to the Northern Hemisphere. Figure 9a also reveals that the success and failures in capturing the observed variations in APO is largely independent of the particular model employed for the inversion.

We now discuss the different model-observation discrepancies, starting with the overprediction of the observed APO at American Samoa (SMO). Figure 9b shows that the simulated high APO concentration at this location is linked to a very strong maximum of APO at the equator that extends symmetrically into both hemispheres (see also Plate 1a). Between $13^\circ N$ and $13^\circ S$ the concentration of APO is predicted to be ~ 10 per meg (per meg refers to the deviation of the measured O_2/N_2 ratio from the O_2/N_2 ratio of a standard multiplied by 1×10^6) higher than poleward of these latitudes. Breaking this maximum down into its components (Figure 9c) reveals that about half of this peak is caused by the equatorial outgassing of O_2 , whereas the other half is caused by the equatorial outgassing of CO_2 (see also Plate 1b). The importance of the CO_2 contribution, which we calculate using Takahashi *et al.*'s [1999] air-sea flux estimates, explains also why the magnitude of this maximum depends only moderately on the OGCM despite the fact that the equatorial O_2 outgassing in SIL(u) is almost twice as large as in the other two models (see Figure 8). Given this small sensitivity and the fact that the observationally based CO_2 fluxes are relatively well constrained [Takahashi *et al.*, 1999], the existence of an equatorial APO maximum appears to be a relatively

robust prediction. However, the magnitude of this maximum is uncertain since it depends on the transport and mixing characteristics of both the oceanic and atmospheric transport models. With regard to the OGCM, the strength of the predicted oxygen outgassing depends on the dynamics of the simulated equatorial upwelling, a process in which coarse-resolution ocean models, such as those employed here, are often deficient [Toggweiler and Carson, 1995; Toggweiler and Samuels, 1993]. Nevertheless, inversions of ocean temperature data with KVLOW(h) resulted in estimated heat fluxes in the equatorial regions that were in good agreement with heat flux climatologies [Gloor *et al.*, this issue], indicating that the inversion results for oxygen are unlikely to be too strongly biased.

The magnitude of the simulated APO signal depends to a considerable degree also on the atmospheric transport model. Atmospheric transport model intercomparison studies [Law *et al.*, 1996; Denning *et al.*, 1999] reveal that the atmospheric transport model used here (GCTM) is relatively sluggish in mixing surface signals into the free troposphere, particularly in the tropics. This results in the generation of substantially larger surface signals for a given flux into the surface boundary layer. Experiments using SF_6 [Denning *et al.*, 1999] and ^{222}Rn indicate that the overprediction of surface signals might be $<30\%$ (S.-M. Fan, unpublished results, 2000). Reducing the simulated APO maximum by this amount would bring it into better agreement with the APO observations at Samoa but would not remove the maximum entirely.

A third possibility that could at least explain a part of the discrepancy is the inability of our inversion to account for the fact that the equatorial oceans are both sources and sinks for atmospheric oxygen. At the axis of upwelling, surface waters are generally undersaturated in oxygen with respect to the atmosphere, leading to an influx of oxygen from the atmosphere. Only as the upwelled waters move poleward as a consequence of Ekman drift do they become supersaturated and thus a source of oxygen to the atmosphere. This latter region dominates the equatorial net flux, but the existence of a small and unconsidered region of oxygen uptake at the equator might reduce the equatorial APO maximum somewhat.

Lacking continuous atmospheric O_2 and CO_2 observations from the equatorial regions, it is currently not possible to evaluate this APO maximum. Stephens [1999] conducted a limited set of observations while crossing the equatorial Pacific several times on a ship during April–May 1998. His preliminary APO data from these crossings indicate slightly higher APO concentrations than found near Cape Kumukahi (KUM) but are inconsistent with the existence of a strong maximum of APO in the equatorial regions. However, these observations were made toward the end of one of the strongest El Niño events observed over the last 100 years. One expects significant changes of tropical APO in response to ENSO events (e.g., outgassing of CO_2 is greatly reduced [Feely *et al.*, 1997, 1999] during warm events), but the timing and magnitude of these changes are not well understood. Therefore long-term observations are needed to better evaluate the model predictions.

The next notable discrepancy between model-simulated APO and observed APO that we discuss is at Cold Bay (CBA), which is located on the Aleutian island chain. The simulation of a substantially higher APO at this site in comparison to the other Northern Hemisphere stations is rather surprising since our inversion estimated the North Pacific to be a sink for oxygen, implying a low APO. Analysis of the different components that contribute to APO in Figure 9c reveals that this surprising result is the consequence of a very strong seasonal APO rectifier effect. As evidenced in Plate 1c, CBA is located at the center of one of the strongest rectifier effects simulated by GCTM on the basis of the seasonal oxygen climatology of Najjar and Keeling [1999] (Plate 1c). Three observations in Plate 1c are notable. First, the seasonal APO rectifier is large, contributing substantially to the spatial APO variability. Second, this rectifier effect is almost everywhere

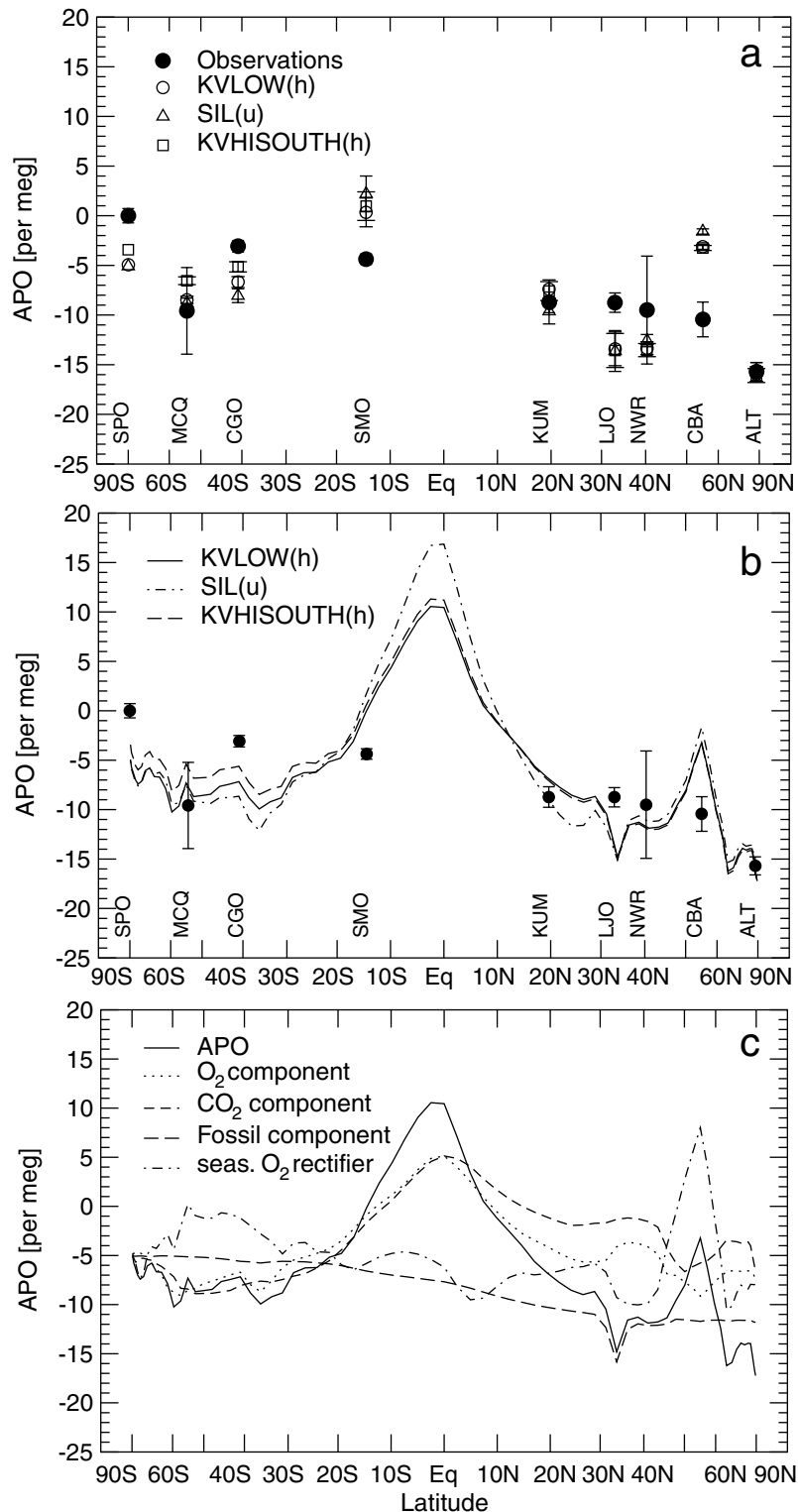


Figure 9. Plots of observed and simulated APO versus latitude. (a) Model-simulated APO using the inversely estimated oxygen and heat fluxes of KVLOW(h), KVHISOUTH(h), and SIL(u) as the lower boundary condition. The solid circles denote the observed APO concentrations at the stations reported by *Stephens et al.* [1998] and updated by *Stephens* [1999]. The open circles, triangles, and squares indicate the model-simulated APO at these stations. (b) Model-simulated APO along a meridional transect in the Pacific Ocean defined by the observation stations. (c) Simulated components of APO for the standard case, KVLOW(h), along the same transect as used in Figure 9b. The three character letters at the bottom denote the observation station: SPO, South Pole Station; MCQ, Macquarie Island; CGO, Cape Grim, Tasmania; SMO, Cape Matatula, American Samoa; KUM: Kumukahi, Hawaii; LJO, La Jolla, California; NWR, Niwot Ridge, Colorado; CBA, Cold Bay, Alaska; ALT, Alert, Northwest Territories.

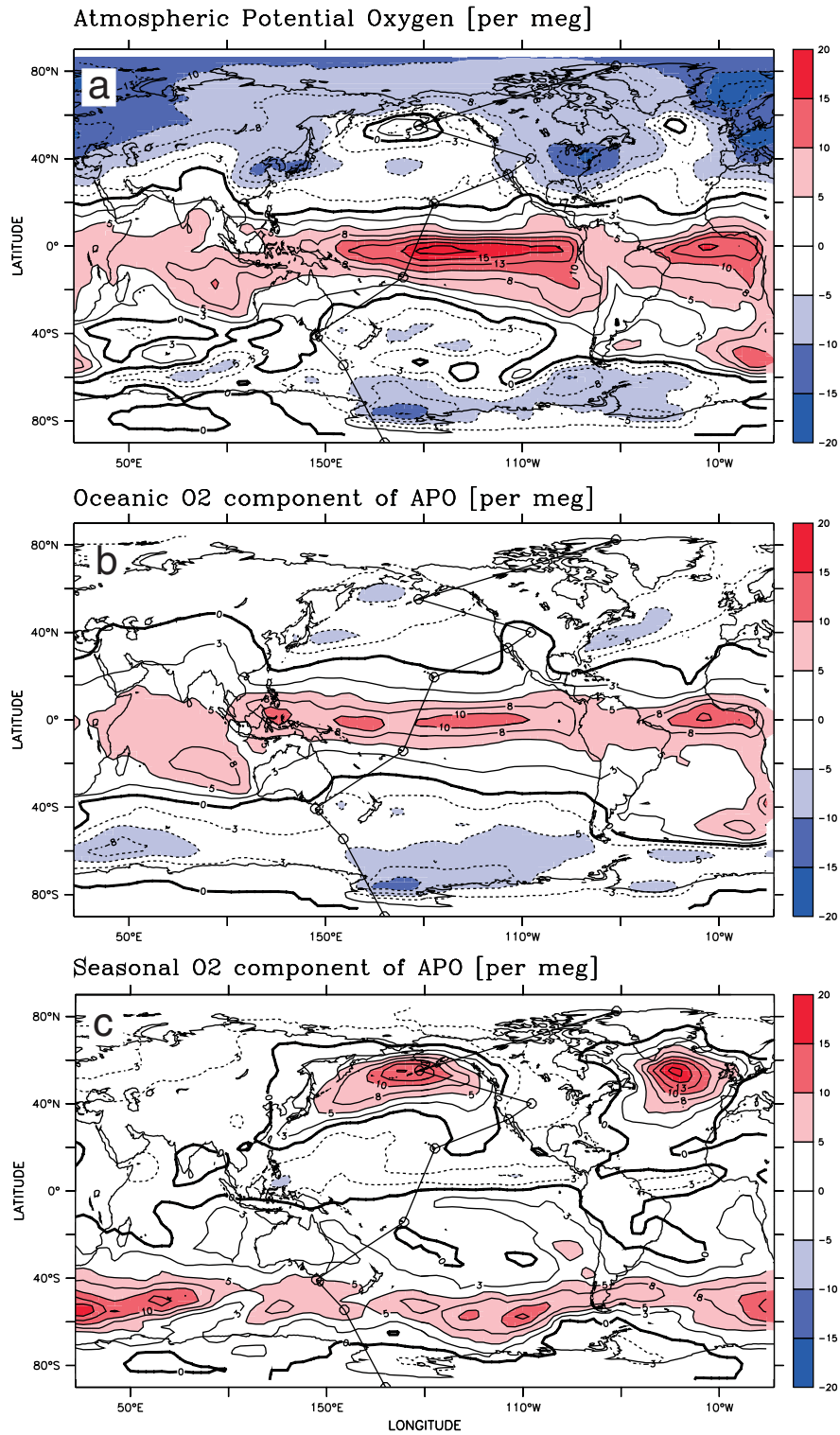


Plate 1. Global maps of model-simulated APO and its components at sea level. (a) Model-simulated APO in per meg on the basis of the inversely estimated oxygen and heat fluxes of KVLW(h) for 13 regions. The circles connected with lines denote the locations of the nine APO observation stations reported by *Stephens et al.* [1998]. (b) The same as Plate 1a, except for the oceanic oxygen component of APO only. (c) The same as Plate 1a, except for the seasonal oxygen rectifier component of APO only.

positive relative to SPO, and third, it is a high-latitude oceanic phenomenon, with its maximum occurring at $\sim 60^\circ$ latitude. Given the importance of this seasonal APO rectifier effect, its causes require better understanding.

Analyses of the seasonal circulation pattern in GCTM and numerical experiments with short-lived tracers indicate that the cause for this seasonal APO rectifier effect is a combination of the covariance between air-sea oxygen fluxes and atmospheric transport and the covariance between the air-sea fluxes and the depth of the atmospheric planetary boundary layer (PBL) [Stephens *et al.*, 1998]. These covariances are greatest at the subpolar latitudes, where strong seasonal variations exist in both oxygen fluxes [Najjar and Keeling [1999], winds [Peixoto and Oort, 1992], and PBL depths. The positive signal is generated by the observation that at these latitudes, oxygen tends to be released from the ocean in summer time, when the lower tropospheric circulation tends to form anticyclonic pattern over the subpolar oceans, thereby trapping the high APO over the ocean. This effect is strengthened by the tendency of the PBL to be shallow in summer time, thereby increasing APO even more. In contrast, in the winter time, when oxygen tends to be taken up by the ocean, the westerly winds tend to blow very zonally over the subpolar oceans, thereby rapidly transporting the low APO signal away from the ocean. At the same time, stronger atmospheric convection over the ocean due to heat release from the ocean surface tends to deepen the PBL in winter-time, further diluting the low APO signal. Thus, over the year, a fixed observation station at these latitudes reports elevated APO concentrations relative to a station where no such covariation occurs since the (high) summertime APO signals are rectified over the (low) wintertime APO signals.

The absence of elevated APO concentrations in the observations at CBA cast doubt on the simulation of this rectifier effect in our atmospheric transport model (GCTM). An overprediction of the simulated seasonal rectifier effect would be consistent with the abovementioned tendency of GCTM to transport surface signals only sluggishly out of the PBL into the free troposphere.

A third discrepancy between model-simulated APO and the observations reported by Stephens *et al.* [1998] is found in the Southern Hemisphere, where we fail to capture the strong meridional variations between Cape Grim, Tasmania (CGO), Macquarie Island (MCQ), and the South Pole station (SPO). As is evident from Plate 1, our simulated APO and its components (especially the rectifier component) exhibit strong spatial variations south of 40°S which are comparable to the observed variations. However, the observation stations are located along a path where the model predicts only relatively little variations, thereby leading to an underprediction of the observed variability. We have relatively little confidence in the correct simulation of the details in the spatial structure of APO and its components, particularly over the Southern Ocean, because of the large uncertainties associated with the spatiotemporal structure of the air-sea flux fields. These uncertainties, particularly with regard to the CO_2 flux fields, stem mostly from relatively poor sample coverage. It is therefore not unlikely that the discrepancy between the model-simulated and observed variations of APO at CGO, MCQ, and SPO is caused by small mismatches between the “real” and modeled air-sea fluxes and atmospheric transport.

The fourth discrepancy between model and observations is the general underestimation of the simulated APO concentration at CGO and SPO relative to the Northern Hemisphere. This is particularly noteworthy since the atmospheric records that went into the reported APO concentration from these stations are among the longest [Stephens *et al.*, 1998]. However, the potential presence of strong rectifier effects at these sites, which are likely not captured by our combination of a priori flux pattern and atmospheric transport model, make a quantitative comparison difficult. It is also possible, however, that our inversion underestimates the net

southward transport of oxygen in the ocean, particularly from the high northern latitudes into the high southern latitudes as discussed below.

Using the inversely estimated heat and oxygen fluxes from the standard case, the atmospheric transport model simulates a difference of ~ 6 per meg in the mean APO concentration between the Southern and Northern Hemispheres (poleward of 13° latitude). This compares well with the observed difference between the two hemispheres of $\sim 8 \pm 3$ per meg (weighted mean). The simulated interhemispheric difference of APO is largely driven by the fossil fuel component of APO (see Figure 9c), but this difference contains also a small oceanic oxygen component. This is the result of the inversion estimating a Northern Hemisphere oxygen sink that is about twice as large as the Southern Hemisphere sink. While the observed mean interhemispheric gradient of APO is well captured by our simulation, our simulated high-latitude difference of ~ 10 per meg is too small relative to the observed APO difference of 16 per meg between station Alert (ALT, 82.5°N) and the South Pole station (SPO, 90°S). Two possible sources for this discrepancy are the underestimation of the APO minimum in the high northern latitudes or the simulation of too low APO in the high southern latitudes. However, both scenarios could, in fact, be linked together if our inversion underestimated the net southward transport of oxygen from the high Northern Hemisphere into the high Southern Hemisphere. While this is a distinct possibility, particularly given the problems associated with deep water formation in the Southern Ocean in most OGCMs [Dutay *et al.*, 2001; Orr *et al.*, 2001], potential biases in atmospheric transport and undersampling of spatial variations in APO need to be considered as well.

In summary, we find that our inversely estimated oxygen fluxes yield atmospheric APO concentrations that generally agree fairly well with direct observations. However, we cannot evaluate yet the most distinct prediction of a strong equatorial maximum of APO because of the lack of long-term observations in this region. Sensitivity studies show that the prediction of this maximum is a consistent feature among all investigated cases, although it is likely that its magnitude has been overestimated because of deficiencies in the oceanic model as well as in the atmospheric model. Independent of this uncertainty, the dominant feature of the oxygen transport in the combined atmosphere-ocean system that emerges from our analysis is the existence of two closed cells in each hemisphere. These cells transport oxygen in the ocean from the high latitudes toward the low latitudes, where it is released to the atmosphere. The cells are closed by transport of oxygen in the atmosphere toward the poles, where the oxygen is then taken up again by the ocean. We find two important asymmetries: The first one involves O_2 uptake in the temperate regions of the Northern Hemisphere versus loss of oxygen in the temperate regions of the Southern Hemisphere. The second asymmetry exists in the Atlantic Ocean, where O_2 is transported southward at all latitudes north of 36°S . The combination of these asymmetries in ocean O_2 transport with the strong latitudinal gradient created from fossil fuel burning leads to an atmospheric APO distribution that is reasonably realistic yet underestimates the observed pole to pole APO gradient. We can thus not exclude the possibility that our inversion underestimates the interhemispheric transport of O_2 . However, the potential existence of large seasonal O_2 rectifier effects and the sparse network of annual APO observations limit the APO constraints on interhemispheric transport.

6. Summary and Conclusions

While the distribution of oxygen in the ocean is relatively well known, estimates of the annual net exchange rates of oxygen

across the air-sea interface are associated with large uncertainties. This is partially caused by the high spatial and temporal variability of the air-sea partial pressure difference that is often not sufficiently resolved by sampling. Additional problems arise because of uncertainties in the parameterization of air-sea gas exchange. We present here the application of a novel inverse modeling technique [Gloor *et al.*, this issue] that avoids these problems and estimates the annual net air-sea flux of oxygen on the basis of its oceanic distribution after correction for biological processes (O_2^*). Our inversion technique is built on three main assumptions. First, it is assumed that the employed OGCM correctly represents the true ocean circulation pathways. Second, we make the assumption that the ocean circulation and oxygen cycles are in steady state, and third, we require that the stoichiometric $O_2:P$ ratio during photosynthesis, respiration and remineralization are constant. Sensitivity studies show that the second and third assumptions introduce little uncertainty but that the inversion results depend to a substantial degree on the quality of the OGCM.

We find that the low latitudes represent strong sources of O_2 to the atmosphere, which is compensated by uptake in the high latitudes, implying an equatorward transport of oxygen in the ocean and a poleward transport of oxygen in the atmosphere. Sensitivity studies with three different OGCMs show that this pattern is relatively robust, although the exact magnitude depends strongly on the simulated ocean circulation. Separation of the inversely estimated O_2 fluxes into thermal (i.e., heat flux driven) and biological components reveals that the air-sea flux pattern is a consequence of a reinforcing tendency of the thermal and biological processes. These results are fully consistent with an analysis of the oceanic distribution of O_2^* and are also independent of the circulation characteristics of the three OGCMs investigated.

Since we assumed steady state, we can integrate the air-sea fluxes in the individual basins and compute meridional transports. In the Atlantic we find a southward oxygen transport of $\sim 83 \text{ Tmol yr}^{-1}$ across 13°N and 26 Tmol yr^{-1} across 13°S . This is the result of a strong oxygen uptake from the atmosphere in the North Atlantic, which exceeds the oxygen release in the equatorial Atlantic. In contrast, no such interhemispheric transport is found in the Indo-Pacific basin since the equatorial outgassing is much stronger than the oxygen uptake in either hemisphere. On a global basis the southward transport of O_2 in the Atlantic across 13°S is more than compensated by 92 Tmol yr^{-1} northward transport across 13°S in the Indo-Pacific, resulting in a northward transport across 13°S . The oceanic oxygen transports implied by the inversely estimated oxygen fluxes are found to be in good agreement with estimates based on hydrographic data, strengthening our confidence in the applicability of our inversion technique.

We further tested our inversely estimated oxygen fluxes by comparing the impact of these fluxes in the atmosphere with observations of atmospheric potential oxygen. For that purpose an atmospheric tracer transport model was run with our annual oxygen fluxes as lower boundary conditions, also including oceanic CO_2 and N_2 fluxes, fossil fuel emission fluxes, and seasonal oceanic O_2 fluxes. The simulated APO agrees relatively well with the observed APO distribution at most observation stations, but the most prominent prediction of the simulation, a strong maximum of APO near the equator, could not be evaluated because of the lack of observations. This maximum was simulated consistently across all sensitivity cases investigated, but it needs to be emphasized that the oceanic and atmospheric models used in this study have a tendency to overestimate its magnitude. Long-term observations of APO in the tropics are urgently needed to better evaluate our predictions and the performance of the employed models.

While our inversely estimated O_2 fluxes resulted in a mean interhemispheric gradient that is close to the observed mean

gradient, our simulated APO significantly underestimates the observed pole to pole APO gradient. While this could be an indication of our underestimating the interhemispheric ocean transport, uncertainties introduced by potentially large oxygen rectifier effects over the ocean and the relatively sparse network of APO observations limit the constraints currently placed by APO on the magnitude of interhemispheric ocean transport. A better characterization of the seasonal oxygen rectification effects and improving the spatial coverage of APO observations particularly in the high-latitudes would provide much improved constraints.

We conclude that our inverse modeling technique provides relatively realistic estimates of the annual net oxygen fluxes across the air-sea interface. It avoids many of the uncertainties associated with direct flux estimates based on air-sea partial pressure differences. However, the results of the oceanic inversion depend to a substantial degree on the OGCM. We investigated three models and found that most conclusions did not change, but these three models are relatively similar in structure and design and therefore might have similar deficiencies. Model intercomparison studies, such as the Ocean Carbon Model Intercomparison Project (OCMIP) [Orr *et al.*, 1997, Orr *et al.*, 2001; Najjar *et al.*, 2001], could provide a means to extend the sensitivity analysis beyond the three models investigated and explore the robustness of the result among a wide range of different OGCMs. It is encouraging that we can expect the quality of the inversion to become better since these models, with the input from OCMIP and other studies, will become more realistic over time.

Acknowledgments. Our thanks go first to the numerous scientists and personnel responsible for the collection, analysis, and handling of the large amount of data that form the basis of our inverse modeling study. We are grateful to R. Keeling, B. Stephens, and M. Bender for valuable and inspiring discussions throughout the course of this study. B. Stephens and R. Keeling are due special thanks for providing their APO data. We thank Ray Najjar for sharing his oxygen climatology. Rick Slater's advice in setting up the ocean general circulation models and providing insight into all problems related to computers was of invaluable help. We thank Anand Gnanadesikan for providing us with his SIL model and for developing the KVLW + ALOW and KVHISOUTH + ALOW models. This work was inspired by a presentation by Y. Yamanaka during his stay at Princeton University. Detailed comments by S. Emerson, B. Stephens, and an anonymous reviewer helped to improve the manuscript. This work was carried out as part of the Carbon Modeling Consortium (CMC), which is supported by the Office of Global Programs of the National Oceanic and Oceanographic Administration. N. Gruber was granted support by a Global and Climate Change fellowship from NOAA. S.-M. Fan was supported by a grant from the Ford Research Laboratory through David Chock. We thank the Geophysical Fluid Dynamics Laboratory and Jerry Mahlman for generously providing computer time. We dedicate this paper to the memory of Tertia Hughes.

References

- Abell, J., S. Emerson, and P. Renaud, Distributions of TOP, TON, and TOC in the North Pacific subtropical gyre: Implications for nutrient supply in the surface ocean and remineralization in the upper thermocline, *J. Mar. Res.*, 58(2), 203–222, 2000.
- Anderson, L. A., and J. L. Sarmiento, Redfield ratios of remineralization determined by nutrient data analysis, *Global Biogeochem. Cycles*, 8(1), 65–80, 1994.
- Augstein, E., N. Bagriantsev, and H. Schenke, Die Expedition ANTARKTIS VIII/1-2, 1989 mit der winter Weddell Gyre Study der Forschungsschiffe *Polarstern* und *Akademik Federov*, *Ber. z. Polarforsch.* 84, Alfred Wegener Inst. Polarforsch., Bremerhaven, Germany, 1991.
- Aumont, O., Étude du cycle naturel du carbone dans un modèle 3d de l'océan mondial, Ph.d. thesis, Univ. Pierre et Marie Curie, Paris, 1998.
- Bainbridge, A., *GEOSECS Atlantic Expedition*, vol. 1, *Hydrographic Data, 1972–1973*, U.S. Govt. Print. Off., Washington, D.C., 1981.

- Battle, M., M. Bender, P. P. Tans, J. W. C. White, J. T. Ellis, T. Conway, and R. J. Francey, Global carbon sinks and their variability, inferred from atmospheric O₂ and δ¹³C, *Science*, 287, 2467–2470, 2000.
- Bender, M., T. Ellis, P. Tans, R. Francey, and D. Lowe, Variability in the O₂/N₂ ratio of Southern Hemisphere air, 1991–1994: Implications for the carbon cycle, *Global Biogeochem. Cycles*, 10(1), 9–21, 1996.
- Bolin, B., and C. D. Keeling, Large-scale atmospheric mixing as deduced from the seasonal and meridional variations of carbon dioxide, *J. Geophys. Res.*, 68, 3899–3920, 1963.
- Boulahdid, M., and J. F. Minster, Oxygen consumption and nutrient regeneration ratios along isopycnal horizons in the Pacific Ocean, *Mar. Chem.*, 26, 133–153, 1989.
- Brewer, P. G., W. S. Broecker, W. J. Jenkins, P. B. Rhines, C. G. Rooth, J. H. Swift, T. Takahashi, and R. T. Williams, A climate freshening of the deep Atlantic north of 50°N over the past 20 years, *Science*, 222, 1237–1239, 1983.
- Broecker, W. S., and T. H. Peng, Gas exchange rates between air and sea, *Tellus*, 26, 21–35, 1974.
- Broecker, W. S., and T.-H. Peng, *Tracers in the Sea*, Lamont-Doherty Earth Observatory, Palisades, N. Y., 1982.
- Broecker, W. S., D. Spencer, and H. Craig, *GEOSECS Pacific Expedition*, vol. 3, *Hydrographic Data, 1973–1974*, U.S. Govt. Print. Off., Washington, D.C., 1982.
- Broecker, W. S., S. Blanton, W. M. Smethie, and G. Ostlund, Radiocarbon decay and oxygen utilization in the deep Atlantic Ocean, *Global Biogeochem. Cycles*, 5(1), 87–117, 1991.
- Caldeira, K., and P. B. Duffy, The role of the Southern Ocean in uptake and storage of anthropogenic carbon dioxide, *Science*, 287, 620–622, 2000.
- Chipman, D., T. Takahashi, D. Breger, and S. Sutherland, Carbon dioxide, hydrographic, and chemical data obtained during the R/V *Meteor* cruise 11/5 in the South Atlantic and Northern Weddell Sea areas (WOCE sections A-12 and A-21), *Data Rep. ORNL/CDIAC-55; NDP-045*, Carbon Dioxide Inf. Anal. Cent., Oak Ridge Natl. Lab., Oak Ridge, Tenn., 1994.
- Chipman, D. W., T. Takahashi, S. Rubin, S. C. Sutherland, and M. H. Koshlyakov, Carbon dioxide, hydrographic, and chemical data obtained during the R/V *Akademik Ioffe* cruise in the South Pacific Ocean (WOCE section S4P, February - April 1992), *Data Rep. ORNL/CDIAC-100; NDP-063*, Carbon Dioxide Inf. Anal. Cent., Oak Ridge Natl. Lab., Oak Ridge, Tenn., 1997.
- Coachman, L. K., and K. Aagaard, Transports through Bering Strait: Annual and interannual variability, *J. Geophys. Res.*, 93, 15,535–15,539, 1988.
- da Silva, A. M., C. C. Young, and S. Levitus, *Atlas of Surface Marine Data 1994*, vol. 1, *Algorithms and Procedures*, NOAA Atlas NESDIS 6, Natl. Oceanic and Atmos. Admin., Silver Spring, Md., 1994.
- Denning, A. S., I. Y. Fung, and D. Randall, Latitudinal gradient of atmospheric CO₂ due to seasonal exchange with land biota, *Nature*, 376, 240–243, 1995.
- Denning, A. S., et al., Three-dimensional transport and concentration of SF₆: A model intercomparison study (TransCom 2), *Tellus, Ser. B.*, 51, 266–297, 1999.
- Deutsch, C. D., N. Gruber, R. M. Key, A. Ganachaud, and J. L. Sarmiento, Denitrification and N₂ fixation in the Pacific Ocean, *Global Biogeochem. Cycles*, 15(2), 483–506, 2001.
- Dutay, J.-C., et al., Evaluation of ocean model ventilation with CFC-11: Comparison of 13 global ocean models, *Ocean Modell.*, in press, 2001.
- Enting, I. G., and J. V. Mansbridge, Latitudinal distribution of sources and sinks of atmospheric CO₂: Direct inversion of filtered data, *Tellus, Ser. B.*, 41, 111–126, 1989.
- Esbensen, S. K., and J. Kushnir, The heat budget of the global oceans: An atlas based on estimates from marine surface observations, *Rep. 29*, Clim. Res. Inst., Oreg. State Univ., Corvallis, 1981.
- Etheridge, D. M., L. P. Steele, R. L. Langenfelds, R. J. Francey, J.-M. Barnola, and V. I. Morgan, Natural and anthropogenic changes in atmospheric CO₂ over the last 1000 years from air in Antarctic ice and firn, *J. Geophys. Res.*, 101, 4115–4128, 1996.
- Fan, S., M. Gloor, J. Mahlman, S. Pacala, J. Sarmiento, T. Takahashi, and P. Tans, A large terrestrial carbon sink in North America implied by atmospheric and oceanic carbon dioxide data and models, *Science*, 282, 442–446, 1998.
- Fan, S.-M., J. L. Sarmiento, M. Gloor, and S. W. Pacala, On the use of regularization techniques in the inverse modeling of atmospheric carbon dioxide, *J. Geophys. Res.*, 104, 21,503–21,512, 1999.
- Feeley, R. A., R. Wanninkhof, C. Goyet, D. E. Archer, and T. Takahashi, Variability of CO₂ distributions and sea-air fluxes in the central and eastern equatorial Pacific during the 1991–1994 El Niño, *Deep Sea Res., Part II*, 44(9–10), 1851–1867, 1997.
- Feeley, R. A., R. Wanninkhof, T. Takahashi, and P. Tans, Influence of El Niño on the equatorial Pacific contribution to atmospheric CO₂ accumulation, *Nature*, 398, 597–601, 1999.
- Forde, E. B., J. C. Hendee, and R. Wanninkhof, Hydrographic, carbon dioxide, nutrient, and productivity measurements from the South Atlantic during July and August of 1991, *Data Rep. ERL AOML-24*, Natl. Oceanic and Atmos. Admin., Silver Spring, Md., 1994.
- Ganachaud, A., Large scale oceanic circulation and fluxes of freshwater, heat, nutrients, and oxygen, Ph.D. thesis, Mass. Inst. of Technol. and Woods Hole Oceanogr. Inst. Joint Program, Boston, 1999.
- Ganachaud, A., and C. Wunsch, Improved estimates of global ocean circulation, heat transport and mixing from new hydrographic measurements, *Nature*, 408, 453–457, 2000.
- Ganachaud, A., C. Wunsch, J. Marotzke, and J. Toole, Meridional overturning and large-scale circulation of the Indian Ocean, *J. Geophys. Res.*, 105, 26,117–26,134, 2000.
- Gent, P. R., J. Willebrand, T. J. McDougall, and J. C. McWilliams, Parameterizing eddy-induced tracer transports in ocean circulation models, *J. Phys. Oceanogr.*, 25, 463–474, 1995.
- Gloor, M., S.-M. Fan, S. W. Pacala, and J. L. Sarmiento, Optimal sampling of the atmosphere for purpose of inverse modeling: A model study, *Global Biogeochem. Cycles*, 14(1), 407–428, 2000.
- Gloor, M., N. Gruber, T. M. C. Hughes, and J. L. Sarmiento, An inverse modeling method for estimation of net air-sea fluxes from bulk data: Methodology and application to the heat cycle, *Global Biogeochem. Cycles*, this issue.
- Gnanadesikan, A., A global model of silicon cycling: Sensitivity to eddy parameterizations and dissolution, *Global Biogeochem. Cycles*, 13(1), 199–220, 1999.
- Gnanadesikan, A., R. D. Slater, N. Gruber, and J. L. Sarmiento, Oceanic vertical exchange and new production: A comparison between models and observations, *Deep Sea Res., Part II*, in press, 2001.
- Goyet, C., P. R. Guenther, C. D. Keeling, and L. D. Talley, Carbon dioxide, hydrographic, and chemical data obtained during the R/V *Thomas Washinton* cruise TUNES 3 in the equatorial Pacific (WOCE section P16C), *Data Rep. ORNL/CDIAC-96; NDP-060*, Carbon Dioxide Inf. Anal. Cent., Oak Ridge Natl. Lab., Oak Ridge, Tenn., 1996.
- Goyet, C., R. M. Key, K. F. Sullivan, and M. Tsuchiya, Carbon dioxide, hydrographic, and chemical data obtained during the R/V *Thomas Washinton* cruise TUNES 1 in the equatorial Pacific (WOCE section P17C), *Data Rep. ORNL/CDIAC-99; NDP-062*, Carbon Dioxide Inf. Anal. Cent., Oak Ridge Natl. Lab., Oak Ridge, Tenn., 1997.
- Graham, N. E., Decadal-scale climate variability in the tropical and North Pacific during the 1970s and 1980s: Observations and model results, *Clim. Dyn.*, 10, 135–162, 1994.
- Gruber, N., and J. L. Sarmiento, Global patterns of marine nitrogen fixation and denitrification, *Global Biogeochem. Cycles*, 11(2), 235–266, 1997.
- Holfort, J., K. M. Johnson, B. Siedler, and D. W. R. Wallace, Meridional transport of dissolved inorganic carbon in the South Atlantic Ocean, *Global Biogeochem. Cycles*, 12(3), 479–499, 1998.
- Indermühle, A., et al., Holocene carbon-cycle dynamics based on CO₂ trapped in ice at Taylor Dome, Antarctica, *Nature*, 398, 121–126, 1999.
- Johnson, G. C., The Pacific Ocean subtropical cell surface limb, *Geophys. Res. Lett.*, 28, 1771–1774, 2001.
- Johnson, K. M., D. W. R. Wallace, R. J. Wilke, and C. Goyet, Carbon dioxide, hydrographic and chemical data obtained during the R/V *Meteor* cruise 15/3 in the South Atlantic ocean (WOCE section A9, February-March 1991), *Data Rep. ORNL/CDIAC-82; NDP-051*, Carbon Dioxide Inf. Anal. Cent., Oak Ridge Natl. Lab., Oak Ridge, Tenn., 1995.
- Johnson, K. M., B. Schneider, L. Mintrop, and D. W. R. Wallace, Carbon dioxide, hydrographic and chemical data obtained during the R/V *Meteor* cruise 18/1 in the North Atlantic Ocean (WOCE section A1E, September 1991), *Data Rep. ORNL/CDIAC-91; NDP-056*, Carbon Dioxide Inf. Anal. Cent., Oak Ridge Natl. Lab., Oak Ridge, Tenn., 1996.
- Karl, D., R. Letelier, L. Tupas, J. Dore, J. Christian, and D. Hebel, The role of nitrogen fixation in the biogeochemical cycling in the subtropical North Pacific Ocean, *Nature*, 388, 533–538, 1997.
- Keeling, C. D., S. C. Piper, and M. Heimann, A three dimensional model of atmospheric CO₂ transport based on observed winds, 4, Mean annual gradients and interannual variations, in *Aspects of Climate Variability in the Pacific and the Western Americas*, *Geophys. Monogr. Ser.*, vol. 55, edited by D. H. Peterson, pp. 305–363, AGU, Washington, D.C., 1989.
- Keeling, R. F., and T.-H. Peng, Transport of heat, CO₂ and O₂ by the Atlantic's thermohaline circulation, *Philos. Trans. R. Soc. London, Ser. B*, 348, 133–142, 1995.
- Keeling, R. F., and S. R. Shertz, Seasonal and interannual variations in atmospheric oxygen and implications for the global carbon cycle, *Nature*, 358, 723–727, 1992.

- Keeling, R. F., G. Najjar, M. L. Bender, and P. P. Tans, What atmospheric oxygen measurements can tell us about the global carbon cycle, *Global Biogeochem. Cycles*, 7(1), 37–67, 1993.
- Keeling, R., S. C. Piper, and M. Heimann, Global and hemispheric CO₂ sinks deduced from changes in atmospheric O₂ concentration, *Nature*, 381, 218–221, 1996.
- Keeling, R. F., B. B. Stephens, R. G. Najjar, S. C. Doney, D. Archer, and M. Heimann, Seasonal variations in the atmospheric O₂/N₂ ratio in relation to the kinetics of air-sea gas exchange, *Global Biogeochem. Cycles*, 12(1), 141–163, 1998.
- Lamb, M. F., R. A. Feely, L. Moore, and D. K. Atwood, Total carbon dioxide, hydrographic, and nitrate measurements in the southwest Pacific during austral autumn, 1990: Results from NOAA/PMEL CGC-90 cruise, *Data Rep. ORNL/CDIAC-84; NDP-052*, Carbon Dioxide Inf. Anal. Cent., Oak Ridge Natl. Lab., Oak Ridge, Tenn., 1995.
- Law, R. M., et al., Variations in modeled atmospheric transport of carbon dioxide and the consequences for CO₂ inversions, *Global Biogeochem. Cycles*, 10(4), 783–796, 1996.
- Lefèvre, N., C. Andrié, Y. Dandonneau, G. Reverdin, and M. Rodier, pCO₂, chemical properties, and estimated new production in the equatorial Pacific in January–March 1991, *J. Geophys. Res.*, 99, 12,639–12,654, 1994.
- Levitus, S., Interpentadal variability of temperature and salinity at intermediate depths of the North Atlantic Ocean, 1970–1974 versus 1955–1959, *J. Geophys. Res.*, 94, 6091–6131, 1989a.
- Levitus, S., Interpentadal variability of temperature and salinity in the deep North Atlantic: 1970–1974 versus 1955–1959, *J. Geophys. Res.*, 94, 16,125–16,131, 1989b.
- Levitus, S., and T. Boyer, *World Ocean Atlas 1994*, vol. 2, *Oxygen*, NOAA Atlas NESDIS 2, Natl. Oceanic and Atmos. Admin., Silver Spring, Md., 1994.
- Liss, P. S., and L. Merlivat, Air-sea exchange rates: Introduction and synthesis, in *The Role of Air-Sea Exchange in Geochemical Cycling*, edited by P. Buat-Ménard, pp. 113–127, D. Reidel, Norwell, Mass., 1986.
- Mahlman, J. D., and W. J. Moxim, Tracer simulation using a global general circulation model: Results from a midlatitude instantaneous source experiment, *J. Atmos. Sci.*, 35, 1340–1374, 1978.
- Marland, G., R. J. Andres, T. A. Boden, C. Johnston, and A. Brenkert, Global, regional and national CO₂ emission estimates from fossil fuel burning, cement production and gas flaring: 1751–1996 (revised August 2000), *Data Rep. ORNL NDP-030*, Carbon Dioxide Inf. Anal. Cent., Oak Ridge Natl. Lab., Oak Ridge, Tenn., 1998.
- Millero, F. J., G. Perron, and J. F. Desnoyers, Heat capacity of seawater solutions from 5°C to 35°C and 0.05 to 22 per mil chlorinity, *J. Geophys. Res.*, 78, 4499–4506, 1973.
- Minster, J., and M. Boulaud, Redfield ratios along isopycnal surfaces: A complementary study, *Deep Sea Res.*, 34, 1981–2003, 1987.
- Najjar, R. G., and R. F. Keeling, Analysis of the mean annual cycle of the dissolved oxygen anomaly in the world ocean, *J. Mar. Res.*, 55, 151–177, 1997.
- Najjar, R., and R. Keeling, The mean annual cycle of the air-sea oxygen flux: A global view, *Global Biogeochem. Cycles*, 14(2), 573–584, 2000.
- Najjar, R., N. Gruber, and J. Orr, Predicting the ocean's response to rising CO₂: The ocean carbon cycle model intercomparison project, *JGOFs Newsl.*, 11(1), 1–4, 2001.
- Oceanographic Data Facility (ODF), South Atlantic Ventilation Experiment (SAVE), chemical, physical and CTD data report, legs 1–3, Scripps Inst. of Oceanogr., La Jolla, Calif., 1992a.
- Oceanographic Data Facility (ODF), South Atlantic Ventilation Experiment (SAVE), chemical, physical and CTD data report, legs 4–5, Scripps Inst. of Oceanogr., La Jolla, Calif., 1992b.
- Orr, J. C., P. Monfray, J. L. Sarmiento, E. Maier-Reimer, J. R. Palmer, and R. G. Najjar, Transition time for ocean carbon-cycle model comparison, *Research GAIM*, 1(2), 1997.
- Orr, J. C., et al., Global oceanic uptake of anthropogenic carbon dioxide as predicted by four 3-D ocean models, *Global Biogeochem. Cycles*, 15(1), 2001.
- Pacanowski, R. C., and S. M. Griffies, Mom 3, version 1: Documentation, user's guide and reference manual, *GFDL Ocean Tech. Rep. 3.4*, Geophys. Fluid Dyn. Lab., Natl. Oceanic and Atmos. Admin., Princeton, N. J., 1998.
- Pahlow, M., and U. Riebesell, Temporal trends in deep ocean Redfield ratios, *Science*, 287, 831–833, 2000.
- Parrilla, G., A. Lavin, H. Bryden, M. Garcia, and R. Millard, Rising temperatures in the subtropical North Atlantic Ocean over the past 35 years, *Nature*, 369, 48–51, 1994.
- Peixoto, J. P., and A. H. Oort, *Physics of Climate*, Am. Inst. of Phys., New York, 1992.
- Physical and Chemical Oceanographic Data Facility (PCODF), C.S.S. Hudson cruise 82-001, 14 February–6 April 1982, *Phys. Chem. Data 84-14*, Scripps Inst. of Oceanogr., La Jolla, 1984.
- Physical and Chemical Oceanographic Data Facility (PCODF), AJAX data report, physical, chemical and in-situ CTD data from the AJAX expedition in the South Atlantic Ocean, Scripps Inst. of Oceanogr., La Jolla, 1985.
- Physical and Chemical Oceanographic Data Facility (PCODF), Transient Tracers in the Ocean: North Atlantic study, *Shipboard Phys. Chem. Data Rep. 86-15*, Scripps Inst. of Oceanogr., La Jolla, Calif., 1986a.
- Physical and Chemical Oceanographic Data Facility (PCODF), Transient Tracers in the Ocean: Tropical Atlantic study, *Shipboard Phys. Chem. Data Rep. 86-16*, Scripps Inst. of Oceanogr., La Jolla, Calif., 1986b.
- Plattner, G.-K., F. Joos, T. F. Stocker, and O. Marchal, Ocean carbon uptake under global warming conditions in a zonally averaged climate model, *Tellus, Ser. B.*, in press, 2001.
- Press, W., S. Teukolsky, W. Vetterling, and B. Flannery, *Numerical Recipes*, 2nd ed., Cambridge Univ. Press, New York, 1992.
- Redfield, A. C., B. H. Ketchum, and F. A. Richards, The influence of organisms on the composition of sea-water, in *The Sea*, edited by M. N. Hill, vol. 2, pp. 26–77, Wiley-Interscience, New York, 1963.
- Roemmich, D., and C. Wunsch, Two trans Atlantic sections: Meridional circulation and heat flux in the subtropical North Atlantic Ocean, *Deep Sea Res.*, 32, 619–665, 1985.
- Rubin, S., J. G. Goddard, D. W. Chipman, T. Takahashi, S. C. Sutherland, J. L. Reid, J. H. Swift, and L. D. Talley, Carbon dioxide, hydrographic, and chemical data obtained in the South Pacific Ocean (WOCE sections P16A/P17A, P17E/P19S, and P19C, R/V Knorr, October 1992–April 1993), *Data Rep. ORNL/CDIAC-109; NDP-065*, Carbon Dioxide Inf. Anal. Cent., Oak Ridge Natl. Lab., Oak Ridge, Tenn., 1998.
- Schmitz, W. J. J., On the interbasin-scale thermohaline circulation, *Rev. Geophys.*, 33(2), 151–173, 1995.
- Severinghaus, J. P., Studies of the terrestrial O₂ and carbon cycles in sand due to gases and in Biosphere 2, Ph.D. thesis, Columbia Univ., New York, 1995.
- Shaffer, G., J. Bendtsen, and O. Ulloa, Fractionation during remineralization of organic matter in the ocean, *Deep Sea Res., Part I*, 46, 185–204, 1999.
- Stephens, B. B., Field-based atmospheric oxygen measurements and the ocean carbon cycle, Ph.D. thesis, Scripps Inst. of Oceanogr., Univ. of Calif., San Diego, La Jolla, 1999.
- Stephens, B. B., R. F. Keeling, M. Heimann, K. D. Six, R. Murnane, and K. Caldeira, Testing global ocean carbon cycle models using measurements of atmospheric O₂ and CO₂ concentration, *Global Biogeochem. Cycles*, 12(2), 213–230, 1998.
- Swift, J. H., N. L. Mantyla, J. R. Osborne, and P. K. Salameh, A transpacific section along 24°N (tps24): Physical, chemical, and CTD data report, 30 March–3 June 1985, R/V Thomas Thompson TT 188 legs 1 and 2, *Tech. Rep. SIO Ref. 90-36*, Scripps Inst. of Oceanogr., La Jolla, Calif., 1990.
- Takahashi, T., W. S. Broecker, and S. Langer, Redfield ratio based on chemical data from isopycnal surfaces, *J. Geophys. Res.*, 90, 6907–6924, 1985.
- Takahashi, T., J. G. Goddard, S. Rubin, D. W. Chipman, S. C. Sutherland, and C. Goyet, Carbon dioxide, hydrographic, and chemical data obtained in the central South Pacific Ocean (WOCE sections P17S and P16S) during the TUNES-2 expedition of the R/V Thomas Washington, July–August, 1991, *Data Rep. ORNL/CDIAC-86; NDP-054*, Carbon Dioxide Inf. Anal. Cent., Oak Ridge Natl. Lab., Oak Ridge, Tenn., 1996.
- Takahashi, T., R. A. Feely, R. Weiss, R. H. Wanninkhof, D. W. Chipman, S. C. Sutherland, and T. T. Takahashi, Global air-sea flux of CO₂: An estimate based on measurements of sea-air pCO₂ difference, in *Revelle Symposium*, edited by C. D. Keeling, *Proc. Natl. Acad. Sci.*, 94, 8292–8299, 1997.
- Takahashi, T., R. H. Wanninkhof, R. A. Feely, R. F. Weiss, D. W. Chipman, N. Bates, J. Olafsson, C. Sabine, and S. C. Sutherland, Net sea-air CO₂ flux over the global oceans: An improved estimate based on the sea-air pCO₂ difference, paper presented at 2nd International Symposium on CO₂ in the Oceans, Natl. Inst. for Environ. Studies, Tsukuba, Japan, 1999.
- Talley, L. D., M. M. Martin, and P. K. Salameh, the Oceanographic Data Facility, Transpacific section in the subpolar gyre (tps47), physical, chemical, and CTD data, R/V Thomas Thompson TT 190, 4 August 1985–7 September 1985, *SIO Ref. 88-9*, Scripps Inst. of Oceanogr., La Jolla, 1988.
- Toggweiler, J. R., and S. Carson, What are upwelling systems contributing to the ocean's carbon and nutrient budgets, in *Upwelling in the Ocean:*

- Modern Processes and Ancient Records*, edited by C. P. Summerhayes et al., pp. 337–360, John Wiley, New York, 1995.
- Toggweiler, J. R., and B. Samuels, New radiocarbon constraints on the upwelling of abyssal water to the ocean's surface, in *The Global Carbon Cycle*, edited by M. Heimann, pp. 333–365. Springer-Verlag, New York, 1993.
- Wanninkhof, R., Relationship between wind speed and gas exchange over the ocean, *J. Geophys. Res.*, *97*, 7373–7382, 1992.
- Wanninkhof, R., and W. R. McGillis, A cubic relationship between air-sea CO₂ exchange and wind speed, *Geophys. Res. Lett.*, *26*(13), 1889–1892, 1999.
- Wanninkhof, R., R. A. Feely, D. K. Atwood, G. Berberian, D. Wilson, P. P. Murphy, and M. F. Lamb, Seasonal and lateral variations in carbon chemistry of surface water in the eastern equatorial Pacific during 1992, *Deep Sea Res., Part II*, *42*, 387–409, 1995.
- Weiss, R., W. Broecker, H. Craig, and D. Spencer, *GEOSECS Indian Ocean Expedition*, vol. 5, *Hydrographic Data 1977–1978*, U.S. Govt. Print. Off., Washington, D.C., 1983.
- Weiss, R. F., The solubility of nitrogen, oxygen and argon in water and seawater, *Deep Sea Res.*, *17*, 721–735, 1970.
- White, W. B., and R. G. Peterson, An Antarctic circumpolar wave in surface pressure, wind, temperature and sea-ice extent, *Nature*, *380*, 699–702, 1996.
- WOCE Hydrographic Program Office, WOCE Indian Ocean data, La Jolla, Calif., 2000.
- WOCE Hydrographic Program Office, Special Analysis Center, WOCE Atlantic leg A16N: Oceanus 202, La Jolla, Calif., 1996a.
- WOCE Hydrographic Program Office, Special Analysis Center, Historical cruises: Oceanus 133-7, La Jolla, Calif., 1996b.
-
- S.-M. Fan and J. L. Sarmiento, Atmospheric and Oceanic Sciences Program, Princeton University, Sayre Hall, Forrestal Campus, P.O. Box CN710, Princeton, NJ 08544-0710, USA. (fan@splash.princeton.edu; jls@splash.princeton.edu)
- M. Gloor, Max Planck Institute for Biogeochemistry, Postfach 100164, D-07701, Jena, Germany. (mgloor@bgc-jena.mpg.de)
- N. Gruber, Department of Atmospheric Sciences and IGPP, 5853 Slichter Hall, University of California, Los Angeles, CA 90095-1567, USA. (ngruber@igpp.ucla.edu)

(Received May 12, 2000; revised March 20, 2001; accepted March 28, 2001.)